

Interferon receptor-deficient mice are susceptible to eschar-associated rickettsiosis

Thomas P. Burke^{1*}, Patrik Engström¹, Cuong J. Tran^{1,2}, Dustin R. Glasner^{2,3}, Diego A. Espinosa^{2,4},
Eva Harris², Matthew D. Welch^{1*}

¹Department of Molecular and Cell Biology, University of California, Berkeley, Berkeley, CA, USA

²Division of Infectious Disease and Vaccinology, School of Public Health, University of California,
Berkeley, Berkeley, CA, USA

³Current address: Department of Laboratory Medicine, University of California, San Francisco, San
Francisco, CA, USA

⁴Current address: Metagenomi, Emeryville, CA, USA

*email: tburke@berkeley.edu; welch@berkeley.edu

1 **Abstract**

2 *Rickettsia* are arthropod-borne pathogens that cause severe human disease worldwide. The
3 spotted fever group (SFG) pathogen *Rickettsia parkeri* elicits skin lesion (eschar) formation in humans
4 after tick bite. However, intradermal inoculation of inbred mice with millions of bacteria fails to elicit
5 eschar formation or disseminated disease, hindering investigations into understanding eschar-
6 associated rickettsiosis. Here, we report that intradermal infection of mice deficient for both interferon
7 receptors (*Ifnar*^{-/-}/*Ifngr*^{-/-}) with *R. parkeri* causes eschar formation, recapitulating the hallmark clinical
8 feature of human disease. Intradermal infection with doses that recapitulate tick infestation caused
9 eschar formation and lethality, including with as few as 10 bacteria. Using this model, we found that the
10 actin-based motility protein Sca2 is required for *R. parkeri* dissemination from the skin to internal organs
11 and for causing lethal disease, and that the abundant *R. parkeri* outer membrane protein OmpB
12 contributes to eschar formation. We also found that immunizing mice with *sca2* and *ompB* mutant *R.*
13 *parkeri* protects against subsequent rechallenge with wild-type bacteria, revealing live-attenuated
14 vaccine candidates. Thus, interferon receptor-deficient mice are a tractable model to investigate
15 rickettsiosis, bacterial virulence factors, and immunity. Our results suggest that differences in interferon
16 signaling in the skin between mice and humans may explain the discrepancy in susceptibility to SFG
17 *Rickettsia*.

18 **Introduction**

19 Obligate cytosolic bacterial pathogens in the family Rickettsiaceae are a diverse group of
20 arthropod-borne microbes that cause severe human disease worldwide, including spotted fever, scrub
21 typhus, and typhus¹⁻³. Human disease caused by the tick-borne spotted fever group (SFG) pathogen
22 *Rickettsia parkeri* is characterized by an eschar at the infection site, generalized rash, headache,
23 fatigue, and fever⁴. There is no approved vaccine for *R. parkeri* or for the more virulent rickettsial
24 pathogens that can cause fatal or latent disease⁵. Moreover, many critical aspects of disease caused
25 by obligate cytosolic bacterial pathogens, including the mechanisms of virulence and immunity, remain
26 unknown, as there are no SFG pathogens that can be handled under biosafety level 2 (BSL2) conditions
27 with corresponding mouse models that recapitulate key features of human disease⁵⁻⁷.

28 *R. parkeri* is genetically similar to the more virulent human pathogens *R. rickettsii* and *R.*
29 *conorii*^{8,9}, and it can be handled under BSL2 conditions. Moreover, mutants can be generated using
30 transposon mutagenesis^{10,11}, and small rodents including mice are natural reservoirs for *R. parkeri*¹²⁻¹⁵.
31 Thus, a mouse model for *R. parkeri* that recapitulates key features of human infection would greatly
32 enhance investigations into understanding rickettsial disease. However, inbred mice including C57BL/6
33 and BALB/c develop no or minor skin lesions upon intradermal (i.d.) infection with millions of *R. parkeri*⁶.
34 C3H/HEJ mice, which harbor a mutation in the gene encoding Toll-like receptor 4 (TLR4), the receptor
35 for extracellular lipopolysaccharide (LPS), have been proposed as models for *R. parkeri*, yet they do
36 not develop disseminated disease and only develop minor skin lesions upon i.d. inoculation⁶. C57BL/6
37 mice have also been proposed as models for *R. parkeri* upon intravenous (i.v.) delivery of 10⁸ bacteria¹⁶.
38 However, this dose is substantially higher than the number of *R. parkeri* found in tick saliva or tick
39 salivary glands¹⁷, and considerable effort is required to generate and concentrate this number of
40 bacteria. An improved mouse model to investigate *R. parkeri* would greatly increase the ability to
41 investigate virulence mechanisms, the host response to infection, and human rickettsial disease.

42 Towards better understanding the host response to *R. parkeri* infection, we recently investigated
43 the relationship between *R. parkeri* and interferons (IFNs), which are ubiquitous signaling molecules of
44 the innate immune system that mobilize the cytosol to an antimicrobial state. Type I IFN (IFN-I) generally

45 restricts viral replication, whereas IFN- γ generally restricts intracellular bacterial pathogens^{18–20}. We
46 observed that mice lacking either gene encoding the receptors for IFN-I (*Ifnar*) or IFN- γ (*Ifngr*) are
47 resistant to i.v. infection with *R. parkeri*, whereas double mutant *Ifnar*^{-/-}*Ifngr*^{-/-} mice succumb²¹. This
48 demonstrates that IFNs redundantly protect against systemic *R. parkeri*. However, the i.v. infection
49 route does not recapitulate eschar formation or mimic the natural route of dissemination. Moreover,
50 *Ifnar*^{-/-}*Ifngr*^{-/-} mice are resistant to i.v. infection with 10^5 bacteria, which may exceed the amount delivered
51 upon tick infestation. Further investigations into whether IFNs redundantly protect against *R. parkeri* in
52 the skin may improve the mouse model for SFG *Rickettsia*.

53 A robust mouse model would allow for more detailed investigations into rickettsial virulence
54 factors. One virulence mechanism shared by divergent cytosolic bacterial pathogens including
55 *Rickettsia*, *Listeria*, *Burkholderia*, *Mycobacterium*, and *Shigella* species, is the ability to undergo actin-
56 based motility, which facilitates cell to cell spread^{22,23}. However, the pathogenic role for many actin-
57 based motility factors *in vivo* remains poorly understood. *R. parkeri* actin-based motility differs from that
58 of other pathogens in that it occurs in two phases, one that requires the RickA protein^{10,24} and the other
59 that requires the Sca2 protein^{10,25}. Only Sca2 is required for efficient cell to cell spread, although it is
60 not required for replication in epithelial cells or for avoiding antimicrobial autophagy^{10,25–27}. *sca2* mutant
61 *R. rickettsii* elicit reduced fever in guinea pigs as compared with wild-type (WT) *R. rickettsii*²⁵, yet the
62 explanation for reduced fever and the pathogenic role for Sca2 *in vivo* remains unclear. Additionally,
63 Sca2 is not essential for dissemination of *R. parkeri* within ticks²⁸. A second virulence strategy employed
64 by intracellular pathogens is the ability to avoid autophagy, which for *R. parkeri* requires outer
65 membrane protein B (OmpB)²⁷. OmpB is important for *R. parkeri* colonization of internal organs in WT
66 mice and for causing lethal disease in IFN receptor-deficient mice after i.v. infection^{21,27}; however, the
67 role for OmpB in *R. parkeri* pathogenesis remains unknown upon i.d. infection. Therefore, unresolved
68 questions remain regarding how Sca2 and OmpB enhance rickettsial pathogenesis.

69 Here, we use IFN receptor-deficient mice to examine the effects of i.d. inoculation of *R. parkeri*,
70 mimicking the natural route of infection. We observe skin lesions that appear similar to human eschars,
71 as well as disseminated lethal disease with as few as 10 bacteria. Using this model, we find that Sca2

72 promotes dissemination and is required for causing lethality, and that OmpB contributes to eschar
73 formation. Finally, we demonstrate that immunization with *sca2* or *ompB* mutant *R. parkeri* protects IFN
74 receptor-deficient mice against subsequent challenge with WT bacteria, revealing live-attenuated
75 vaccine candidates. Our study establishes a mouse model to investigate numerous aspects of
76 *Rickettsia* pathogenesis, including eschar formation, virulence factors, and immunity. More broadly, this
77 work also reveals that a potent, redundant IFN response protects mice from eschar-associated
78 rickettsiosis.

79 **Results**

80 **I.d. infection of *Ifnar*^{-/-}/*Ifngr*^{-/-} mice causes lethal disease and skin lesions that are grossly similar
81 to human eschars.**

82 Although i.v. delivery can recapitulate an immediate systemic disease for many pathogens, it
83 does not mimic the natural route of infection for tick-borne pathogens. In contrast, i.d. delivery better
84 mimics the natural route of infection and allows for investigations into dissemination from the initial
85 infection site to internal organs. We therefore sought to develop an i.d. murine infection model to better
86 recapitulate the natural route of tick-borne *R. parkeri* infection. WT, *Tlr4*^{-/-}, *Ifnar*^{-/-}, *Ifngr*^{-/-}, and *Ifnar*^{-/-}/*Ifngr*
87 ^{-/-} C57BL/6J mice, as well as outbred CD-1 mice, were infected i.d. with 10⁷ WT *R. parkeri* and monitored
88 over time. No or minor dermal lesions appeared at the site of infection in WT, *Tlr4*^{-/-}, *Ifnar*^{-/-}, or *Ifngr*
89 ^{-/-} C57BL/6J mice or CD-1 mice (**Fig. 1a**, **Fig. S1a**). In contrast, double mutant *Ifnar*^{-/-}/*Ifngr*^{-/-} C57BL/6J
90 mice developed large necrotic skin lesions (**Fig. 1b**) that appeared grossly similar to human eschars
91 (**Fig. 1c**). In some cases, tails of *Ifnar*^{-/-}/*Ifngr*^{-/-} or *Ifngr*^{-/-} mutant mice became inflamed after i.d. or i.v.
92 infection (**Fig. S1b**). These findings demonstrate that interferons redundantly control disease caused
93 by *R. parkeri* in the skin and that i.d. infection of *Ifnar*^{-/-}/*Ifngr*^{-/-} mice recapitulates the hallmark
94 manifestation of human disease caused by *R. parkeri*.

95 Our previous observations using the i.v. route revealed dose-dependent lethality in *Ifnar*^{-/-}/*Ifngr*
96 ^{-/-} mice, with 10⁷ *R. parkeri* eliciting 100% lethality and 10⁵ *R. parkeri* eliciting no lethality²¹. *R. parkeri* are
97 present in tick saliva at a concentration of approximately 10⁴ per 1 µl, and approximately 10⁷ *R. parkeri*
98 are found in tick salivary glands¹⁷. However, the number of bacteria delivered from tick infestation likely
99 varies depending on many factors, and we therefore sought to examine the effects of different doses of
100 *R. parkeri* upon i.d. infection of *Ifnar*^{-/-}/*Ifngr*^{-/-} mice. We observed skin lesion formation at all infectious
101 doses, from 10⁷ to 10 bacteria (**Fig. 1d**), suggesting that i.d. infection of *Ifnar*^{-/-}/*Ifngr*^{-/-} mice elicits lesions
102 with doses similar to what is delivered by tick infestation.

103 We next sought to quantitatively evaluate the effects of i.d. infection by monitoring animal weight,
104 body temperature, the degree of lesion formation, and lethality. Intradermally-infected *Ifnar*^{-/-}/*Ifngr*^{-/-} mice
105 lost significant body weight (**Fig. 2a**; **Fig. S2a**) and body temperature (**Fig. 2b**; animals were euthanized

106 when body temperature fell below 90° F / 32.2° C) as compared with WT mice, whereas infected *Tlr4*^{-/-}
107 , *Ifnar*^{-/-}, *Ifngr*^{-/-} mice did not. To evaluate lesion severity, we scored lesions upon infection with different
108 doses of *R. parkeri*. Whereas 10⁷ bacteria elicited similar responses as 10⁵, 10⁴, 10³, and 10² bacteria
109 (**Fig. 2c**), lesions were less severe when mice were infected with 10¹ bacteria compared with 10⁷
110 bacteria. If mice survived, lesions healed over the course of approximately 15-40 days post infection
111 (d.p.i.) at all doses (**Fig. S2b**).

112 To investigate whether i.d. infection by *R. parkeri* caused lethal disease, we monitored mouse
113 survival over time. Upon i.d. delivery of 10⁷ *R. parkeri*, 8 of 12 *Ifnar*^{-/-}*Ifngr*^{-/-} mice exhibited lethargy,
114 paralysis, or body temperatures below 90° F, at which point they were euthanized, whereas delivery of
115 the same dose of bacteria to WT and single mutant mice did not elicit lesions and all survived (**Fig. 2d**).
116 Lower doses of *R. parkeri* also elicited body weight loss (**Fig. 2a**), body temperature loss (**Fig. S2c**),
117 and lethal disease (**Fig. 2d**) in *Ifnar*^{-/-}*Ifngr*^{-/-} mice. The cause of lethality in this model remains unclear
118 and will require further investigation. Nevertheless, these findings reveal that i.d. infection can cause
119 lethal disease in *Ifnar*^{-/-}*Ifngr*^{-/-} mice with ~10,000-fold lower dose of bacteria than i.v. infection.

120 It remained unclear whether i.d. infection could also be used to model dissemination from the
121 skin to internal organs. We therefore evaluated bacterial burdens in spleens and livers of WT and *Ifnar*
122 ^{-/-}*Ifngr*^{-/-} mice at 5 d.p.i. by measuring *R. parkeri* plaque-forming units (p.f.u.). Bacteria were not
123 recoverable from spleens and livers of intradermally-infected WT mice, suggesting that they did not
124 disseminate from the skin to internal organs in high numbers (**Fig. 2e**). In contrast, bacteria were
125 recovered from spleens and livers of intradermally-infected *Ifnar*^{-/-}*Ifngr*^{-/-} mice at 5 d.p.i. (**Fig. 2e**). This
126 demonstrates that i.d. infection of *Ifnar*^{-/-}*Ifngr*^{-/-} mice with *R. parkeri* causes systemic infection and can
127 be used as a model for dissemination from the skin to internal organs.

128

129 ***Ifnar*^{-/-}*Ifngr*^{-/-} mice do not succumb to intradermal infection with *sca2* mutant *R. parkeri*.**

130 Sca2 mediates actin-based motility in rickettsial pathogens; however, its contribution to virulence
131 *in vivo* remains unclear. We examined if i.v. and i.d. infections of WT and *Ifnar*^{-/-}*Ifngr*^{-/-} mice could reveal
132 a pathogenic role for *R. parkeri* Sca2. Upon i.v. infection with 5 x 10⁶ bacteria (**Fig. 3a**) or 10⁷ bacteria

133 (**Fig. 3b**), we observed that *sca2*::Tn mutant *R. parkeri* caused reduced lethality compared to WT
134 bacteria. Similarly, i.d. infection with *sca2*::Tn mutant bacteria elicited significantly less lethality (**Fig.**
135 **3c**) and weight loss (**Fig. 3d**) as compared to WT bacteria and no severe temperature loss (**Fig. S3a**).
136 Although we sought to evaluate infection using a *sca2* complement strain of *R. parkeri*, our attempts to
137 generate such a strain were unsuccessful. As an alternative strategy, we examined whether the
138 transposon insertion itself had an effect on *R. parkeri* survival *in vivo*. We evaluated infection of an *R.*
139 *parkeri* strain that harbors a transposon insertion in *MC1_RS08740* (previously annotated as
140 *MC1_05535*), which has no known role in virulence²⁷. I.v. infection with *MC1_RS08740*::Tn *R. parkeri*
141 caused lethality to a similar degree as WT *R. parkeri* (**Fig. 3a**), demonstrating that the transposon likely
142 does not significantly impact *R. parkeri* fitness *in vivo*. Together, these findings suggest that the actin-
143 based motility factor Sca2 is required for causing lethal disease in *Ifnar*^{-/-}*Ifngr*^{-/-} mice.

144

145 ***Ifnar*^{-/-}*Ifngr*^{-/-} mice exhibit similar skin lesion formation and vascular damage upon i.d. infection
146 with WT and *sca2*::Tn *R. parkeri*.**

147 We next examined whether Sca2 facilitates *R. parkeri* dissemination throughout the skin and
148 whether Sca2 is required for lesion formation. Unexpectedly, upon i.d. inoculation, *Ifnar*^{-/-}*Ifngr*^{-/-} mice
149 infected with *sca2*::Tn mutant bacteria developed skin lesions that were of similar severity to lesions
150 caused by WT *R. parkeri*; however, the lesions elicited by *sca2* mutant bacteria appeared significantly
151 earlier than lesions caused by WT bacteria (**Fig. 3e**). Further examinations will be required to better
152 evaluate this observation; however, it may suggest that actin-based motility enables *R. parkeri* to avoid
153 a rapid onset of inflammation in the skin. To evaluate *R. parkeri* dissemination within the skin, we used
154 a fluorescence-based assay that measures vascular damage as a proxy for pathogen dissemination²⁹.
155 Mice were intradermally infected with WT and *sca2*::Tn *R. parkeri*. At 5 d.p.i., fluorescent dextran was
156 intravenously delivered, and fluorescence was measured at the infection site (**Fig. 3f**, representative
157 small black circle) and in the surrounding area (**Fig. 3f**, representative large black circle). No significant
158 differences were observed when comparing WT and *sca2*::Tn *R. parkeri* infections in *Ifnar*^{-/-}*Ifngr*^{-/-} mice
159 using an infectious dose of 10⁷ *R. parkeri* in the larger surrounding area (**Fig. 3g**) or at the site of

160 infection (**Fig. S4a**). Similar results were observed upon infection with 10^6 or 10^5 bacteria (**Fig. S4b,c**).
161 However, significantly more fluorescence was observed in the skin of infected *Ifnar*^{-/-}/*Ifngr*^{-/-} mice as
162 compared to WT mice (**Fig. 3g**), demonstrating that interferons protect against increased vascular
163 permeability during *R. parkeri* infection. Together, the gross pathological analysis and fluorescence-
164 based assay suggest that Sca2 likely does not significantly enhance *R. parkeri* dissemination in the skin
165 during i.d. infection of *Ifnar*^{-/-}/*Ifngr*^{-/-} mice.

166

167 ***R. parkeri* Sca2 promotes dissemination from the skin to spleens and livers.**

168 Among the factors that mediate actin-based motility, the *L. monocytogenes* actin-based motility
169 factor ActA is one of the best understood. ActA enables *L. monocytogenes* to spread from cell to cell^{22,23},
170 escape antimicrobial autophagy³⁰⁻³³, proliferate in mouse organs after i.v. infection^{34,35}, and cause lethal
171 disease in mice^{36,37}. We initially hypothesized that *R. parkeri* Sca2 plays a similar pathogenic role *in*
172 *vivo* to ActA, which we found is required for bacterial survival in spleens and livers upon i.v. delivery
173 (**Fig. 3h**), in agreement with previous experiments^{34,35}. However, when we examined bacterial burdens
174 upon i.v. infection of *Ifnar*^{-/-}/*Ifngr*^{-/-} mice with *R. parkeri*, similar amounts of WT and *sca2*::Tn bacteria
175 were recovered in spleens (**Fig. 3i**). We were also surprised to find that significantly more *sca2*::Tn than
176 WT *R. parkeri* were recovered in livers (**Fig. 3i**). The explanation for higher *sca2*::Tn burdens in livers
177 remains unclear. Nevertheless, these data reveal that Sca2 is likely not essential for *R. parkeri* survival
178 in blood, invasion of host cells, or intracellular survival in spleens and livers.

179 We next evaluated the role for Sca2 in *R. parkeri* dissemination by measuring p.f.u. in spleens
180 and livers following i.d. infection of *Ifnar*^{-/-}/*Ifngr*^{-/-} mice. After i.d. infection, *sca2*::Tn mutant bacteria were
181 ~20-fold reduced in their abundance in spleens and ~2-fold reduced in their abundance in livers as
182 compared to WT *R. parkeri* (**Fig. 3j**). Similar results were seen upon i.d. infection with lower doses of
183 *sca2*::Tn and WT bacteria (**Fig. 3k**). Together, these results suggest that Sca2 is required for *R. parkeri*
184 dissemination from the skin to internal organs.

185

186 ***R. parkeri* actin-based motility does not contribute to avoiding innate immunity *in vitro*.**

187 Sca2-mediated actin-based motility is required for efficient plaque formation and cell to cell
188 spread by *R. parkeri* *in vitro*^{10,25}. However, it remains unclear if Sca2 enables *R. parkeri* to escape
189 detection or restriction by innate immunity. The actin-based motility factor ActA enables *L.*
190 *monocytogenes* to avoid autophagy^{32,33}, and the antimicrobial guanylate binding proteins (GBPs) inhibit
191 *Shigella flexneri* actin-based motility³⁸. We therefore sought to evaluate whether Sca2-mediated actin-
192 based motility enables *R. parkeri* to evade innate immunity *in vitro*. We found that the *sca2*::Tn mutant
193 grew similarly to WT bacteria in endothelial cells (**Fig. S5a**), consistent with previous reports in epithelial
194 cells^{10,25}. We also examined whether Sca2 contributed to *R. parkeri* survival or growth in bone marrow-
195 derived macrophages (BMDMs), which can restrict other *R. parkeri* mutants that grow normally in
196 endothelial cells²⁷. However, no significant difference in bacterial survival was observed between WT
197 and *sca2*::Tn bacteria in BMDMs in the presence or absence of IFN- β (**Fig. S5b**). WT and *sca2* mutant
198 *R. parkeri* also elicited similar amounts of host cell death (**Fig. S5c**) and IFN-I production (**Fig. S5d**).
199 Moreover, we found that the anti-rickettsial factor GBP2 localized to the surface of *sca2*::Tn mutant *R.*
200 *parkeri* at similar frequency as with WT bacteria in the presence or absence of IFN- β (**Fig. S5e,f**).
201 Together, these data suggest that Sca2 does not significantly enhance the ability of *R. parkeri* to evade
202 innate immunity *in vitro*.

203

204 ***Ifnar*^{-/-}*Ifngr*^{-/-} mice exhibit less severe skin lesions upon infection with a highly attenuated *R.*
205 *parkeri* mutant.**

206 Because *sca2* mutant *R. parkeri* showed no defect in eschar formation compared to WT, it
207 remained unclear whether skin lesion formation in *Ifnar*^{-/-}*Ifngr*^{-/-} mice was influenced by bacterial
208 virulence factors. We therefore investigated i.d. infection with *ompB*::Tn^{STOP} *R. parkeri*, which harbors
209 both a transposon and a stop codon in *ompB*²⁷, and is severely attenuated *in vivo*^{21,27}. In contrast with
210 WT bacteria, i.d. infection of *Ifnar*^{-/-}*Ifngr*^{-/-} mice with *ompB*::Tn^{STOP} *R. parkeri* caused no lethality (**Fig.**
211 **4a**) or reduced weight loss (**Fig. 4b**). The *ompB*::Tn^{STOP} mutant *R. parkeri* also caused significantly less
212 severe skin lesions than WT bacteria (**Fig. 4c**). These findings suggest that *Ifnar*^{-/-}*Ifngr*^{-/-} mice can be
213 used as a model to identify bacterial genes important for eschar formation.

214

215 **Immunizing *Ifnar*^{-/-}*Ifngr*^{-/-} mice with attenuated *R. parkeri* mutants protects against subsequent**
216 **rechallenge.**

217 There is currently no available vaccine to protect against SFG *Rickettsia*, which can cause
218 severe and lethal human disease^{5,39}, and investigations into identifying live attenuated vaccine
219 candidates has been hindered by the lack of robust animal models. We therefore examined whether
220 immunization with attenuated *R. parkeri* mutants would protect against subsequent re-challenge with a
221 lethal dose of WT bacteria. *Ifnar*^{-/-}*Ifngr*^{-/-} mice were immunized i.v. with 5×10^6 *sca2::Tn* or *ompB::Tn*^{STOP}
222 *R. parkeri* and 40 d later were intravenously re-challenged with 10^7 WT *R. parkeri*, which is
223 approximately 10-times a 50% lethal dose (LD₅₀)²¹. All mice immunized with *sca2* or *ompB* mutant *R.*
224 *parkeri* survived, whereas all naïve mice succumbed by 6 d.p.i. (Fig. 5a). Upon rechallenge, mice
225 immunized with *ompB* and *sca2* mutants also did not lose significant weight (Fig. 5b) or body
226 temperature (Fig. 5c). These data indicate that attenuated *R. parkeri* mutants elicit a robust protective
227 immune response, and that *Ifnar*^{-/-}*Ifngr*^{-/-} mice may serve as tools to develop live attenuated *R. parkeri*
228 vaccine candidates.

229

230 **Discussion**

231 In this study, we show that IFN-I and IFN- γ redundantly protect inbred mice from eschar-
232 associated rickettsiosis and disseminated disease by *R. parkeri*. Eschar formation is the hallmark
233 clinical feature of human disease caused by *R. parkeri*⁴, and thus these findings suggest that the striking
234 difference between human and mouse susceptibilities to *R. parkeri* may be due to IFN signaling in the
235 skin. Using this mouse model, we uncover a role for *R. parkeri* Sca2 in dissemination, for OmpB in skin
236 lesion formation, and for both proteins in causing lethal disease. We further demonstrate that attenuated
237 *R. parkeri* mutants elicit long-lasting immunity, revealing live attenuated vaccine candidates. Obligate
238 cytosolic bacterial pathogens cause a variety of severe human diseases on six continents^{1,40}, and the
239 animal model described here will facilitate future investigations into *R. parkeri* virulence factors, the host

240 response to infection, the molecular determinants of human disease, and propagation of tick-borne
241 pathogens in wildlife reservoirs.

242 Our finding that i.d. infection of *Ifnar*^{-/-}*Ifngr*^{-/-} mice causes eschar formation, the hallmark of *R.*
243 *parkeri* infection in humans⁴, may indicate that the human IFN response is less well adapted to control
244 *R. parkeri* than in mice. Future investigations into the IFN-stimulated genes that restrict *R. parkeri* in
245 mouse versus human cells may improve our understanding of human susceptibility to SFG *Rickettsia*.
246 Additionally, our findings that OmpB promotes eschar formation demonstrates that *Ifnar*^{-/-}*Ifngr*^{-/-} mice
247 can be used to identify bacterial factors that are important for human disease manifestations. More
248 broadly, investigating the IFN response in the skin may lead us to better understand diseases caused
249 by other arthropod-borne pathogens. One example may be *Orientia tsutsugamushi*, the causative agent
250 of scrub typhus⁴¹, a prevalent but poorly understood tropical disease endemic to Southeast Asia^{1,42,43}.
251 *O. tsutsugamushi* also causes eschar formation in humans, but inbred mice do not recapitulate eschar
252 formation during *O. tsutsugamushi* infection⁷, similar to *R. parkeri*. A second example may be *Borrelia*
253 *burgdorferi*, a tick-borne pathogen that causes a skin rash at the site of tick bite as a hallmark feature
254 of Lyme disease⁴⁴, the most prevalent tick-borne disease in the United States^{44,45}. Existing mouse
255 models also do not recapitulate skin rash formation following *B. burgdorferi* infection^{46,47}. Further
256 investigations into how IFNs protect the skin in mice may therefore reveal aspects of human disease
257 caused by other arthropod-borne pathogens.

258 Our study further highlights the utility of mouse models that mimic natural routes of infection.
259 Infection via the i.v. and intraperitoneal (i.p.) routes can mimic systemic disease, yet these are unnatural
260 routes for many microbes, including food-borne, arthropod-borne, or aerosol-borne pathogens. Our
261 observation that i.d. infection can cause lethal disease with as few as 10 bacteria, ~10,000 fewer
262 bacteria than i.v. infection²¹, suggests that *R. parkeri* may be highly adapted to reside in the skin.
263 However, this model could be further improved by investigating the role for tick vector components in
264 pathogenesis. Saliva from ticks, mosquitos, and sand flies enhances pathogenesis of arthropod-borne
265 bacterial, viral, and parasitic pathogens^{48–50}, and non-human primates inoculated with *R. parkeri* exhibit
266 altered inflammatory responses when administered after tick-bite⁵¹. This may suggest a potential role

267 for tick vector components such as tick saliva in *R. parkeri* pathogenesis. Developing improved murine
268 infection models that mimic the natural route of infection, including with tick saliva or the tick vector, is
269 critical to better understand the virulence and transmission of tick-borne pathogens.

270 Many *Rickettsia* species, as well as many facultative cytosolic pathogens including *L.*
271 *monocytogenes*, undergo actin-based motility to spread from cell to cell. For *L. monocytogenes*, the
272 actin-based motility factor ActA enables the pathogen to survive *in vivo*, as *actA* mutant bacteria are
273 over 1,000-fold attenuated by measuring lethality^{36,37} and by enumerating bacteria in spleens and livers
274 of mice after i.v. infection^{34,35}. However, the pathogenic role for actin-based motility in the Rickettsiae
275 has remained unclear. We find that Sca2 is not required for intracellular survival in organs upon i.v.
276 infection of *Ifnar*^{-/-}*Ifngr*^{-/-} mice, but rather, is required for dissemination from skin to internal organs and
277 lethality upon i.d. infection. Consistent with an important role for Sca2 in pathogenesis, a previous study
278 reported that i.v. infection of guinea pigs with *sca2* mutant *R. rickettsii* did not elicit fever²⁵. Our results
279 suggest that Sca2-mediated actin-based motility by *Rickettsia* may facilitate dissemination in host
280 reservoirs, although we cannot rule out other roles for Sca2 that do not involve actin assembly. *R.*
281 *prowazekii* and *R. typhi*, which cause severe human disease, encode a fragmented *sca2* gene⁵², and
282 undergo no or dramatically reduced frequency of actin-based motility, respectively^{53,54}. Although it
283 remains unclear why some *Rickettsia* species lost the ability to undergo actin-based motility, Sca2 is
284 dispensable for *R. parkeri* dissemination in the tick vector²⁸, suggesting that actin-based motility may
285 play a specific role in dissemination within mammalian hosts.

286 We find that *sca2* or *ompB* mutant *R. parkeri* elicit a robust protective immune response in *Ifnar*
287 ^{-/-}*Ifngr*^{-/-} mice. These findings complement previous observations that *sca2* mutant *R. rickettsii* elicits
288 antibody responses in guinea pigs²⁵, and expands upon these findings by demonstrating protection from
289 rechallenge and revealing additional vaccine candidates. There are currently limited vaccine candidates
290 that protect against rickettsial disease⁵. Identifying new vaccine candidates may reveal avenues to
291 protect against tick-borne infections and aerosolized *Rickettsia*, which are extremely virulent and
292 potential bioterrorism agents⁵⁵, as well as against Brill-Zinsser disease, caused by latent *R. prowazekii*⁵.
293 Future studies exploring whether attenuated *R. parkeri* mutants provide immunity against other

294 *Rickettsia* species are warranted to better define the mechanisms of protection. These findings on
295 immunity may also help develop *R. parkeri* as an antigen delivery platform. *R. parkeri* resides directly
296 in the host cytosol for days and could potentially be engineered to secrete foreign antigens for
297 presentation by major histocompatibility complex I. In summary, the mouse model described here will
298 facilitate future investigations into numerous aspects of *R. parkeri* infection, including actin-based
299 motility and immunity, and may serve as model for other arthropod-borne pathogens.

300 **Methods**

301 **Bacterial preparations**

302 *R. parkeri* strain Portsmouth was originally obtained from Dr. Christopher Paddock (Centers for
303 Disease Control and Prevention). To amplify *R. parkeri*, confluent monolayers of female African green
304 monkey kidney epithelial Vero cells (obtained from UC Berkeley Cell Culture Facility, tested for
305 mycoplasma contamination, and authenticated by mass spectrometry) were infected with 5×10^6 *R.*
306 *parkeri* per T175 flask. Vero cells were grown in DMEM (Gibco 11965-092) containing 4.5 g l⁻¹ glucose
307 and 2% fetal bovine serum (FBS; GemCell). Infected cells were scraped and collected at 5 or 6 d.p.i.
308 when ~90% of cells were rounded due to infection. Scrapped cells were then centrifuged at 12,000g for
309 20 min at 4°C. Pelleted cells were resuspended in K-36 buffer (0.05 M KH₂PO₄, 0.05 M K₂HPO₄, 100
310 mM KCl, 15 mM NaCl, pH 7) and dounced for ~40 strokes at 4°C. The suspension was then centrifuged
311 at 200g for 5 min at 4°C to pellet host cell debris. Supernatant containing *R. parkeri* was overlaid on a
312 30% MD-76R (Merry X-Ray) gradient solution in ultracentrifuge tubes (Beckman/Coulter Cat 344058).
313 Gradients were centrifuged at 18,000 r.p.m. in an SW-28 ultracentrifuge swinging bucket rotor
314 (Beckman/Coulter) for 20 min at 4°C. These '30% prep' bacterial pellets were resuspended in brain
315 heart infusion (BHI) media (BD, 237500), aliquoted, and stored at -80°C. Titers were determined by
316 plaque assays by serially diluting the *R. parkeri* in 6-well plates containing confluent Vero cells. Plates
317 were spun for 5 min at 300g in an Eppendorf 5810R centrifuge and at 24 h post infection (h.p.i.); the
318 media from each well was aspirated, and the wells were overlaid with 4 ml/well DMEM with 5% FBS
319 and 0.7% agarose (Invitrogen, 16500-500). At 6 d.p.i., an overlay of 0.7% agarose in DMEM containing
320 2.5% neutral red (Sigma, N6264) was added. Plaques were then counted 24 h later. For infections with
321 *ompB* mutant bacteria, the *ompB*^{STOP::Tn} mutant was used, which contains a transposon and an
322 upstream stop codon in *ompB*, as previously described²⁷.

323

324 **Deriving bone marrow macrophages**

325 For obtaining bone marrow, male or female mice were euthanized, and femurs, tibias, and
326 fibulas were excised. Bones were sterilized with 70% ethanol and washed with BMDM media (20% FBS

327 (HyClone), 0.1% β -mercaptoethanol, 1% sodium pyruvate, 10% conditioned supernatant from 3T3
328 fibroblasts, in DMEM (Gibco) with 4.5 g $^{-1}$ glucose and 100 μ g/ml streptomycin and 100 U/ml penicillin),
329 and ground with a mortar and pestle. Bone homogenate was passed through a 70 μ m nylon cell strainer
330 (Thermo Fisher Scientific, 08-771-2) for particulate removal. Filtrates were then centrifuged at 290g in
331 an Eppendorf 5810R centrifuge for 8 min, supernatant was aspirated, and the pellet was resuspended
332 in BMDM media. Cells were plated in 30 ml BMDM media in non-TC-treated 15 cm petri dishes at a
333 ratio of 10 dishes per 2 femurs/tibias and incubated at 37° C. An additional 30 ml of BMDM media was
334 added 3 d later. At 7 d the media was aspirated, 15 ml cold PBS (Gibco, 10010-023) was added, and
335 cells were incubated at 4° C with for 10 min. BMDMs were scraped from the plate, collected in a 50 ml
336 conical tube, and centrifuged at 290g for 5 min. PBS was aspirated, and cells were resuspended in
337 BMDM media with 30% FBS and 10% DMSO at 10 7 cells/ml. 1 ml aliquots were stored at -80° C for 24
338 h in Styrofoam boxes and then moved to long-term storage in liquid nitrogen.

339

340 **Infections *in vitro***

341 HMEC-1 cells (obtained from the UC Berkeley Cell Culture Facility and authenticated by short-
342 tandem-repeat analysis) were passaged 2-3 times weekly and grown at 37° C with 5% CO₂ in DMEM
343 containing 10 mM L-glutamine (Sigma, M8537), supplemented with 10% heat-inactivated FBS
344 (HyClone), 1 μ g/mL hydrocortisone (Spectrum Chemical, CO137), 10 ng/mL epidermal growth factor
345 (Thermo Fisher Scientific, CB40001; Corning cat. no. 354001), and 1.18 mg/mL sodium bicarbonate.
346 HMEC media was prepared every 1-2 months, and aliquoted and stored at 4° C. To prepare HMEC-1
347 cells for infection, cells were treated with 0.25% trypsin-EDTA (Thermo Fisher Scientific); the number
348 of cells was counted using a hemocytometer (Bright-Line), and 3 \times 10 4 cells were plated into 24-well
349 plates 48 h prior to infection.

350 To plate macrophages for infection, BMDM aliquots were thawed on ice, diluted into 9 ml of
351 DMEM, centrifuged at 290g for 5 min in an Eppendorf 5810R centrifuge, and the pellet was resuspended
352 in 10 ml BMDM media without antibiotics. 5 \times 10 5 cells were plated into 24-well plates. Approximately
353 16 h later, “30% prep” *R. parkeri* were thawed on ice and diluted into fresh BMDM media to either 10 6

354 p.f.u./ml or 2×10^5 p.f.u./ml. Media was then aspirated from the BMDMs, replaced with 500 μ l media
355 containing *R. parkeri*, and plates were spun at 300g for 5 min in an Eppendorf 5810R centrifuge.
356 Infected cells were incubated in a humidified CEDCO 1600 incubator set to 33°C and 5% CO₂.
357 Recombinant mouse IFN- β (PBL, 12405-1) was added directly to infected cells after spinfection.

358 For measuring p.f.u., supernatants from infected BMDMs were aspirated, and each well was
359 washed twice with 500 μ l sterile milli-Q-grade water. After adding 1 ml of sterile milli-Q water to each
360 well, macrophages were lysed by repeated pipetting. Serial dilutions of lysates were added to confluent
361 Vero cells in 12 well plates. Plates were spun at 300g using an Eppendorf 5810R centrifuge for 5 min
362 at room temperature and incubated at 33°C overnight. At ~16 h.p.i., media was aspirated and replaced
363 with 2 ml/well of DMEM containing 0.7% agarose and 5% FBS (GemCell). At ~6 d.p.i., 1 ml of DMEM
364 containing 0.7% agarose, 1% FBS (GemCell), 200 μ g/ml amphotericin B (Invitrogen, 15290-018), and
365 2.5% neutral red (Sigma) was added to each well. Plaques were then counted after 24 h.

366 Microscopy, LDH, and IFN-I experiments were performed as described²¹.

367

368 Animal experiments

369 Animal research was conducted under a protocol approved by the University of California,
370 Berkeley Institutional Animal Care and Use Committee (IACUC) in compliance with the Animal Welfare
371 Act and other federal statutes relating to animals and experiments using animals (Welch lab animal use
372 protocol AUP-2016-02-8426). The University of California, Berkeley IACUC is fully accredited by the
373 Association for the Assessment and Accreditation of Laboratory Animal Care International and adheres
374 to the principles of the Guide for the Care and use of Laboratory Animals⁵⁶. Mouse infections were
375 performed in a biosafety level 2 facility. All animals were maintained at the University of California,
376 Berkeley campus, and all infections were performed in accordance with the approved protocols. Mice
377 were between 8 and 20 weeks old at the time of initial infection. Mice were selected for experiments
378 based on their availability, regardless of sex. The sex of mice used for survival after i.d. infection and
379 raw data for mouse experiments is indicated in **Supplemental Table 1**. A statistical analysis was not
380 performed to predetermine sample size prior to initial experiments. Initial sample sizes were based on

381 availability of mice and the capacity to process or measure samples within a given time. After the first
382 experiment, a Power Analysis was conducted to determine subsequent group sizes. All mice were of
383 the C57BL/6J background, except for outbred CD-1 mice. All mice were healthy at the time of infection
384 and were housed in microisolator cages and provided chow, water, and bedding. No mice were
385 administered antibiotics or maintained on water with antibiotics. Experimental groups were littermates
386 of the same sex that were randomly assigned to experimental groups. For experiments with mice
387 deficient in *Ifnar* and *Ifngr*, mice were immediately euthanized if they exhibited severe degree of
388 infection, as defined by a core body temperature dropping below 90° F or lethargy that prevented normal
389 movement.

390

391 **Mouse genotyping**

392 *Tlr4*^{-/-}⁵⁷, *Ifnar*^{-/-}⁵⁸, *Ifngr*^{-/-}⁵⁹, *Ifnar*^{-/-}*Ifngr*^{-/-} and WT C57BL/6J mice were previously described and
393 originally obtained from Jackson Laboratories. CD-1 mice were obtained from Charles River. For
394 genotyping, ear clips were boiled for 15 min in 60 µl of 25 mM NaOH, quenched with 10 µl Tris-HCl pH
395 5.5, and 2 µl of lysate was used for PCR using SapphireAMP (Takara, RR350) and gene-specific
396 primers. Primers used were: *Ifnar* forward (F): CAACATACTACAACGACCAAGTGTG; *Ifnar* WT
397 reverse (R): AACAAACCCCCAAACCCCAG; *Ifnar*^{-/-} R: ATCTGGACGAAGAGCATCAGG; *Ifngr* (F):
398 CTCGTGCTTACGGTATCGC; *Ifngr* (R): TCGCTTCCAGCTGATGTACT; WT *Tlr4* (F):
399 CACCTGATACTTAATGCTGGCTGTAAAAAG; WT *Tlr4* (R):
400 GGTTTAGGCCAGAGTTTGTCTTCA; *Tlr4*^{-/-} (F): TGTTGCCCTCAGTCACAGAGACTCTG;
401 and *Tlr4*^{-/-} (R): TGTTGGTCGTTGTCGGATCCGTCG.

402

403 **Mouse infections**

404 For mouse infections, *R. parkeri* was prepared by diluting 30%-prep bacteria into cold sterile
405 PBS on ice. Bacterial suspensions were kept on ice during injections. For i.d. infections, mice were
406 anaesthetized with 2.5% isoflurane via inhalation. The right flank of each mouse was shaved with a hair
407 trimmer (Braintree CLP-41590), wiped with 70% ethanol, and 50 µl of bacterial suspension in PBS was

408 injected intradermally using a 30.5-gauge needle. Mice were monitored for ~3 min until they were fully
409 awake. No adverse effects were recorded from anesthesia. For i.v. infections, mice were exposed to a
410 heat lamp while in their cages for approximately 5 min and then each mouse was moved to a mouse
411 restrainer (Braintree, TB-150 STD). The tail was sterilized with 70% ethanol, and 200 μ l of bacterial
412 suspension in sterile PBS was injected using 30.5-gauge needles into the lateral tail vein. Body
413 temperatures were monitored using a rodent rectal thermometer (BrainTree Scientific, RET-3).

414 For fluorescent dextran experiments, mice were intravenously injected with 150 μ l of 10 kDa
415 dextran conjugated with Alexa Fluor 680 (D34680; Thermo Fisher Scientific) at a concentration of 1
416 mg/ml in sterile PBS²⁹. As a negative control, mice with no *R. parkeri* infection were injected with
417 fluorescent dextran. As an additional negative control, uninfected mice were injected intravenously with
418 PBS instead of fluorescent dextran. At 2 h post-injection, mice were euthanized with CO₂ and cervical
419 dislocation, doused with 70% ethanol, and skin surrounding the injection site (approximately 2 cm in
420 each direction) was removed. Connective tissue between the skin and peritoneum was removed, and
421 skin was placed hair-side-up on a 15 cm Petri dish. Skin was imaged with an LI-COR Odyssey CLx (LI-
422 COR Biosciences), and fluorescence was quantified using ImageStudioLite v5.2.5. The skin from mice
423 with no injected fluorescent dextran was used as the background measurement. Skin from mice injected
424 with fluorescent dextran but no *R. parkeri* was normalized to an arbitrary number (100), and *R. parkeri*-
425 infected samples were normalized to this value (*R. parkeri*-infected / uninfected X 100). The number of
426 pixels at the injection site area was maintained across experiments (7,800 for small area and 80,000
427 for the large area).

428 All mice in this study were monitored daily for clinical signs of disease throughout the course of
429 infection, such as hunched posture, lethargy, scruffed fur, paralysis, facial edema, and lesions on the
430 skin of the flank and tail. If any such manifestations were observed, mice were monitored for changes
431 in body weight and temperature. If a mouse displayed severe signs of infection, as defined by a
432 reduction in body temperature below 90°F or an inability to move normally, the animal was immediately
433 and humanely euthanized using CO₂ followed by cervical dislocation, according to IACUC-approved
434 procedures. Pictures of skin and tail lesions were obtained with permission from the Animal Care and

435 Use Committee Chair and the Office of Laboratory and Animal Care. Pictures were captured with an
436 Apple iPhone 8, software v13.3.1.

437 For harvesting spleens and livers, mice were euthanized at the indicated pre-determined times
438 and doused with ethanol. Mouse organs were extracted and deposited into 50 ml conical tubes
439 containing 4 ml sterile cold PBS for the spleen and 8 ml PBS for the liver. Organs were kept on ice and
440 were homogenized for ~10 s using an immersion homogenizer (Fisher, Polytron PT 2500E) at ~22,000
441 r.p.m. Organ homogenates were spun at 290g for 5 min to pellet the cell debris (Eppendorf 5810R
442 centrifuge). 20 μ l of organ homogenates were then serial diluted into 12-well plates containing confluent
443 Vero cells. The plates were then spun at 260g for 5 min at room temperature (Eppendorf 5810R
444 centrifuge) and incubated at 33°C. To reduce the possibility of contamination, organ homogenates were
445 plated in duplicate and the second replicate was treated with 50 μ g/ml carbenicillin (Sigma) and 200
446 μ g/ml amphotericin B (Gibco). The next day, at approximately 16 h.p.i., the cells were gently washed
447 by replacing the existing media with 1 ml DMEM containing 2% FBS (GemCell). The media were then
448 aspirated and replaced with 2 ml/well of DMEM containing 0.7% agarose, 5% FBS, and 200 μ g/ml
449 amphotericin B. When plaques were visible at 6 d.p.i., 1 ml of DMEM containing 0.7% agarose, 1%
450 FBS, and 2.5% neutral red (Sigma) was added to each well, and plaques were counted at 24 h.p.i.

451

452 **Statistical analysis**

453 Statistical parameters and significance are reported in the figure legends. For comparing two
454 sets of data, a two-tailed Student's T test was performed. For comparing two sets of *in vivo* p.f.u. data,
455 Mann-Whitney *U* tests were used. For comparing two survival curves, log-rank (Mantel-Cox) tests were
456 used. For comparing curves of two samples (mouse health, weight, and temperature), two-way
457 ANOVAs were used. For two-way ANOVAs, if a mouse was euthanized prior to the statistical endpoint,
458 the final value that was recorded for the mouse was repeated until the statistical endpoint. For two-way
459 ANOVAs, if a measurement was not recorded for a timepoint, the difference between values at adjacent
460 time points was used. Data were determined to be statistically significant when $P<0.05$. Asterisks
461 denote statistical significance as: * $P<0.05$; ** $P<0.01$; *** $P<0.001$; **** $P<0.0001$, compared to indicated

462 controls. Error bars indicate standard deviation (SD) for *in vitro* experiments and standard error of the
463 mean (SEM) for *in vivo* experiments. All other graphical representations are described in the figure
464 legends. Statistical analyses were performed using GraphPad PRISM v7.0.

465

466 **Data availability**

467 WT and *ompB* mutant *R. parkeri* were authenticated by whole genome sequencing and are
468 available in the NCBI Trace and Short-Read Archive; Sequence Read Archive (SRA), accession
469 numbers: SRX4401164 (WT) and SRX4401167 (*ompB*::Tn^{STOP}). Raw Data for figures in the main text
470 are available in **Supplemental Table 1**.

471

472 **Competing interests**

473 The authors declare no competing interests.

474

475 **Author contributions**

476 T.P.B. performed and analyzed experiments. C.J.T., P.E., D.R.G., and D.A.E. contributed to
477 performing experiments and provided reagents. T.P.B. wrote the original draft of this manuscript with
478 guidance from M.D.W. Critical reading and edits of the manuscript were provided by C.J.T., P.E., and
479 M.D.W. Supervision was provided by T.P.B. and M.D.W.

480

481 **Acknowledgements**

482 We thank Neil Fisher for editing this manuscript. P.E. was supported by postdoctoral fellowships
483 from the Sweden-America Foundation. M.D.W. was supported by NIH/NIAID grants R01AI109044 and
484 R21AI138550. D.R.G., D.A.E., and E.H. were partially supported by NIH/NIAID grant R01 AI24493
485 (E.H.).

486 **Bibliography**

487 1. Bonell, A., Lubell, Y., Newton, P. N., Crump, J. A. & Paris, D. H. Estimating the burden of scrub
488 typhus: A systematic review. *PLoS Negl. Trop. Dis.* **11**, e0005838 (2017).

489 2. Fang, R., Blanton, L. S. & Walker, D. H. Rickettsiae as Emerging Infectious Agents. *Clinics in*
490 *Laboratory Medicine* vol. 37 383–400 (2017).

491 3. Sahni, A., Fang, R., Sahni, S. K. & Walker, D. H. Pathogenesis of Rickettsial Diseases:
492 Pathogenic and Immune Mechanisms of an Endotheliotropic Infection. *Annu. Rev. Pathol.*
493 *Mech. Dis.* **14**, 127–152 (2019).

494 4. Paddock, C. D. *et al.* Rickettsia parkeri Rickettsiosis and Its Clinical Distinction from Rocky
495 Mountain Spotted Fever. *Clin. Infect. Dis.* **47**, 1188–1196 (2008).

496 5. Osterloh, A. Immune response against rickettsiae: lessons from murine infection models. *Med.*
497 *Microbiol. Immunol.* **206**, 403–417 (2017).

498 6. Grasperge, B. J. *et al.* Susceptibility of inbred mice to Rickettsia parkeri. *Infect. Immun.* **80**,
499 1846–1852 (2012).

500 7. Sunyakumthorn, P. *et al.* An Intradermal Inoculation Model of Scrub Typhus in Swiss CD-1
501 Mice Demonstrates More Rapid Dissemination of Virulent Strains of Orientia tsutsugamushi.
502 *PLoS One* **8**, (2013).

503 8. Roux, V. & Raoult, D. Phylogenetic analysis of members of the genus Rickettsia using the gene
504 encoding the outer-membrane protein rOmpB (ompB). *Int. J. Syst. Evol. Microbiol.* **50**, 1449–
505 1455 (2000).

506 9. Goddard, J. Historical and recent evidence for close relationships among Rickettsia parkeri, R.
507 conorii, R. africae, and R. sibirica: Implications for rickettsial taxonomy. *J. Vector Ecol.* **34**, 238–
508 242 (2009).

509 10. Reed, S. C. O., Lamason, R. L., Risca, V. I., Abernathy, E. & Welch, M. D. Rickettsia actin-
510 based motility occurs in distinct phases mediated by different actin nucleators. *Curr. Biol.* **24**,
511 98–103 (2014).

512 11. Lamason, R. L., Kafai, N. M. & Welch, M. D. A streamlined method for transposon mutagenesis

513 of *Rickettsia parkeri* yields numerous mutations that impact infection. *PLoS One* **13**, 1–12
514 (2018).

515 12. Moraru, G. M. *et al.* Evidence of antibodies to spotted fever group rickettsiae in small mammals
516 and quail from Mississippi. *Vector-Borne Zoonotic Dis.* **13**, 1–5 (2013).

517 13. Moraru, G. M., Goddard, J., Paddock, C. D. & Varela-Stokes, A. Experimental infection of
518 cotton rats and bobwhite quail with *Rickettsia parkeri*. *Parasites and Vectors* **6**, 1–5 (2013).

519 14. Krawczak, F. S. *et al.* Ecology of a tick-borne spotted fever in southern Brazil. *Exp. Appl.*
520 *Acarol.* **70**, 219–229 (2016).

521 15. Barbieri, A. R. M. *et al.* Species richness and seasonal dynamics of ticks with notes on
522 rickettsial infection in a Natural Park of the Cerrado biome in Brazil. *Ticks Tick. Borne. Dis.* **10**,
523 442–453 (2019).

524 16. Londoño, A. F., Mendell, N. L., Walker, D. H. & Bouyer, D. H. A biosafety level-2 dose-
525 dependent lethal mouse model of spotted fever rickettsiosis: *Rickettsia parkeri* atlantic
526 rainforest strain. *PLoS Negl. Trop. Dis.* **13**, e0007054 (2019).

527 17. Suwanbongkot, C. *et al.* Spotted fever group rickettsia infection and transmission dynamics in
528 *Amblyomma maculatum*. *Infect. Immun.* **87**, e00804-18 (2019).

529 18. Raniga, K. & Liang, C. Interferons: Reprogramming the metabolic network against viral
530 infection. *Viruses* **10**, 1–21 (2018).

531 19. Billiau, A. & Matthys, P. Interferon- γ : A historical perspective. *Cytokine and Growth Factor*
532 *Reviews* vol. 20 97–113 (2009).

533 20. Meunier, E. & Broz, P. Interferon-inducible GTPases in cell autonomous and innate immunity.
534 *Cell. Microbiol.* **18**, 168–180 (2016).

535 21. Burke, T. P. *et al.* Inflammasome-mediated antagonism of type I interferon enhances *Rickettsia*
536 pathogenesis. *Nat. Microbiol.* **5**, 688–696 (2020).

537 22. Choe, J. E. & Welch, M. D. Actin-based motility of bacterial pathogens: mechanistic diversity
538 and its impact on virulence. *Pathog. Dis.* **74**, ftw099 (2016).

539 23. Lamason, R. L. & Welch, M. D. Actin-based motility and cell-to-cell spread of bacterial

540 pathogens. *Current Opinion in Microbiology* vol. 35 48–57 (2017).

541 24. Jeng, R. L. *et al.* A Rickettsia WASP-like protein activates the Arp2/3 complex and mediates
542 actin-based motility. *Cell. Microbiol.* **6**, 761–769 (2004).

543 25. Kleba, B., Clark, T. R., Lutter, E. I., Ellison, D. W. & Hackstadt, T. Disruption of the Rickettsia
544 rickettsii Sca2 autotransporter inhibits actin-based motility. *Infect. Immun.* **78**, 2240–2247
545 (2010).

546 26. Haglund, C. M., Choe, J. E., Skau, C. T., Kovar, D. R. & Welch, M. D. Rickettsia Sca2 is a
547 bacterial formin-like mediator of actin-based motility. *Nat. Cell Biol.* **12**, 1057–1063 (2010).

548 27. Engström, P. *et al.* Evasion of autophagy mediated by Rickettsia surface protein OmpB is
549 critical for virulence. *Nat. Microbiol.* **4**, 2538–2551 (2019).

550 28. Harris, E. K. *et al.* Role of Sca2 and RickA in the dissemination of Rickettsia parkeri in
551 Amblyomma maculatum. *Infect. Immun.* **86**, e00123-18 (2018).

552 29. Glasner, D. R. *et al.* Dengue virus NS1 cytokine-independent vascular leak is dependent on
553 endothelial glycocalyx components. *PLoS Pathog.* **13**, 1–22 (2017).

554 30. Cheng, M. I., Chen, C., Engström, P., Portnoy, D. A. & Mitchell, G. Actin-based motility allows
555 Listeria monocytogenes to avoid autophagy in the macrophage cytosol. *Cell. Microbiol.* **20**,
556 e12854 (2018).

557 31. Mitchell, G. *et al.* Listeria monocytogenes triggers noncanonical autophagy upon phagocytosis,
558 but avoids subsequent growth-restricting xenophagy. *Proc. Natl. Acad. Sci. U. S. A.* **115**, E210–
559 E217 (2017).

560 32. Yoshikawa, Y. *et al.* Listeria monocytogenes ActA-mediated escape from autophagic
561 recognition. *Nat. Cell Biol.* **11**, 1233–1240 (2009).

562 33. Yoshikawa, Y., Ogawa, M., Hain, T., Chakraborty, T. & Sasakawa, C. Listeria monocytogenes
563 ActA is a key player in evading autophagic recognition. *Autophagy* **5**, 1220–1221 (2009).

564 34. Auerbuch, V., Lenz, L. L. & Portnoy, D. A. Development of a competitive index assay to
565 evaluate the virulence of Listeria monocytogenes actA mutants during primary and secondary
566 infection of mice. *Infect. Immun.* **69**, 5953–5957 (2001).

567 35. Le Monnier, A. *et al.* ActA is required for crossing of the fetoplacental barrier by Listeria
568 moncytogenes. *Infect. Immun.* **75**, 950–957 (2007).

569 36. Goossens, P. L., Milon, G. & Bevan, M. Induction of protective CD8+ T lymphocytes by an
570 attenuated listeria moncytogenes actA mutant. *Int. Immunol.* **4**, 1413–1418 (1992).

571 37. Brundage, R. A., Smith, G. A., Camilli, A., Theriot, J. A. & Portnoy, D. A. Expression and
572 phosphorylation of the Listeria moncytogenes actA protein in mammalian cells. *Proc. Natl.*
573 *Acad. Sci. U. S. A.* **90**, 11890–11894 (1993).

574 38. Piro, A. S. *et al.* Detection of cytosolic shigella flexneri via a C-terminal triple-arginine motif of
575 GBP1 inhibits actin-based motility. *MBio* **8**, e01979-17 (2017).

576 39. Dantas-Torres, F. Rocky Mountain spotted fever. *Lancet Infectious Diseases* vol. 7 724–732
577 (2007).

578 40. Abdad, M. Y., Abdallah, R. A., Fournier, P. E., Stenos, J. & Vasoo, S. A concise review of the
579 epidemiology and diagnostics of rickettsioses: Rickettsia and orientia spp. *Journal of Clinical*
580 *Microbiology* vol. 56 e01728-17 (2018).

581 41. Rajapakse, S., Weeratunga, P., Sivayoganathan, S. & Fernando, S. D. Clinical manifestations
582 of scrub typhus. *Transactions of the Royal Society of Tropical Medicine and Hygiene* vol. 111
583 43–54 (2017).

584 42. Kelly, D. J., Foley, D. H. & Richards, A. L. A Spatiotemporal Database to Track Human Scrub
585 Typhus Using the VectorMap Application. *PLoS Neglected Tropical Diseases* vol. 9 e0004161
586 (2015).

587 43. Richards, A. L. & Jiang, J. Scrub typhus: Historic perspective and current status of the
588 worldwide presence of Orientia species. *Tropical Medicine and Infectious Disease* vol. 5 49
589 (2020).

590 44. Bratton, R. L., Whiteside, J. W., Hovan, M. J., Engle, R. L. & Edwards, F. D. Diagnosis and
591 treatment of lyme disease. *Mayo Clinic Proceedings* vol. 83 566–571 (2008).

592 45. Schwartz, A. M., Hinckley, A. F., Mead, P. S., Hook, S. A. & Kugeler, K. J. Surveillance for lyme
593 disease - United States, 2008-2015. *MMWR Surveill. Summ.* **66**, (2017).

594 46. Barthold, S. W., Beck, D. S., Hansen, G. M., Terwilliger, G. A. & Moody, K. D. Lyme borreliosis
595 in selected strains and ages of laboratory mice. *J. Infect. Dis.* **162**, 133–138 (1990).

596 47. Wang, G. *et al.* Impact of genotypic variation of *Borrelia burgdorferi* sensu stricto on kinetics of
597 dissemination and severity of disease in C3H/HeJ mice. *Infect. Immun.* **69**, 4303–4312 (2001).

598 48. Pingen, M., Schmid, M. A., Harris, E. & McKimmie, C. S. Mosquito Biting Modulates Skin
599 Response to Virus Infection. *Trends in Parasitology* vol. 33 645–657 (2017).

600 49. Lestinova, T., Rohousova, I., Sima, M., de Oliveira, C. I. & Volf, P. Insights into the sand fly
601 saliva: Blood-feeding and immune interactions between sand flies, hosts, and *Leishmania*.
602 *PLoS Negl. Trop. Dis.* **11**, e0005600 (2017).

603 50. Šimo, L., Kazimirova, M., Richardson, J. & Bonnet, S. I. The essential role of tick salivary
604 glands and saliva in tick feeding and pathogen transmission. *Front. Cell. Infect. Microbiol.* **7**,
605 281 (2017).

606 51. Banajee, K. H. *et al.* *Amblyomma maculatum* feeding augments *Rickettsia parkeri* infection in a
607 rhesus macaque model: A pilot study. *PLoS One* **10**, 1–20 (2015).

608 52. Ngwamidiba, M., Blanc, G., Ogata, H., Raoult, D. & Fournier, P. E. Phylogenetic study of
609 *Rickettsia* species using sequences of the autotransporter protein-encoding gene *sca2*. *Ann. N.*
610 *Y. Acad. Sci.* **1063**, 94–99 (2005).

611 53. Teyssiere, N., Chiche-Portiche, C. & Raoult, D. Intracellular movements of *Rickettsia conorii*
612 adn *R. typhi* based on actin polymerization. *Res. Microbiol.* **143**, 821–829 (1992).

613 54. Heinzen, R. A., Hayes, S. F., Peacock, M. G. & Hackstadt, T. Directional actin polymerization
614 associated with spotted fever group *Rickettsia* infection of Vero cells. *Infect. Immun.* **61**, 1926–
615 1935 (1993).

616 55. Walker, D. H. The realities of biodefense vaccines against *Rickettsia*. *Vaccine* **27**, D52-55
617 (2009).

618 56. National Research Council. *Guide for the Care and Use of Laboratory Animals. The*
619 *Biochemical journal.* (2010).

620 57. Hoshino, K. *et al.* Cutting edge: Toll-like receptor 4 (TLR4)-deficient mice are hyporesponsive

621 to lipopolysaccharide: evidence for TLR4 as the Lps gene product. *J. Immunol.* **162**, 3749–52

622 (1999).

623 58. Müller, U. *et al.* Functional role of type I and type II interferons in antiviral defense. *Science (80-*

624 *.)*. **264**, 1918–1921 (1994).

625 59. Huang, S. *et al.* Immune response in mice that lack the interferon- γ receptor. *Science (80-.)*.

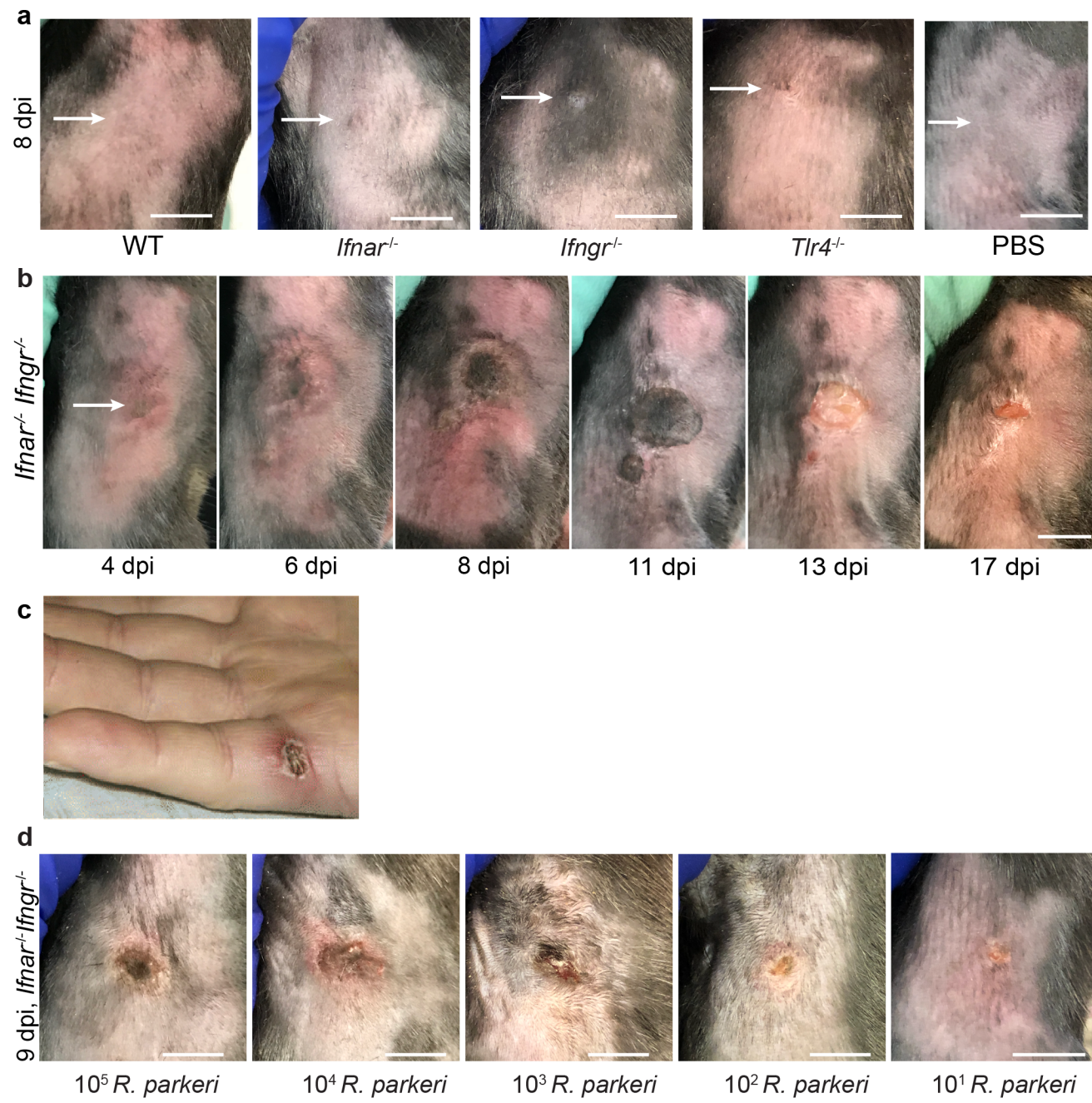
626 **259**, 1742–1745 (1993).

627

628

629
630

Figures



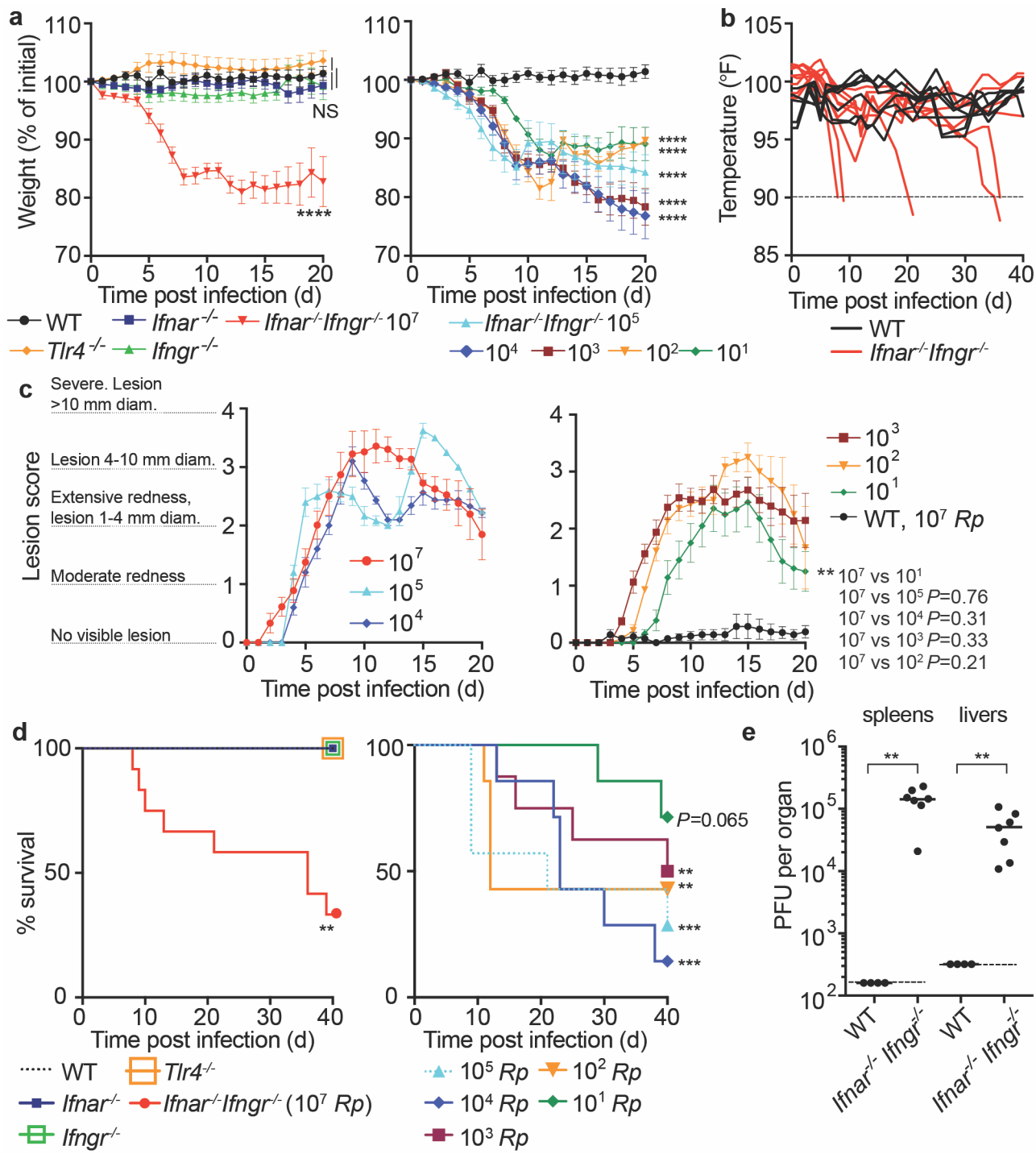
631

632
633

Figure 1: I.d. infection of *Ifnar^{-/-}Ifngr^{-/-}* mice with *R. parkeri* elicits skin lesions that are grossly similar to human eschars.

634
635
636
637
638
639
640
641

a) Representative images of WT, *Ifnar^{-/-}*, *Ifngr^{-/-}*, and *Tlr4^{-/-}* mice, infected intradermally with 10⁷ WT *R. parkeri* at 8 dpi and WT mice injected with PBS. White arrows indicate the infection site on the right flank of the mouse. Scale bar, 1 cm. Data are representative of three independent experiments. b) Representative images of an *Ifnar^{-/-}Ifngr^{-/-}* mouse after i.d. inoculation with 10⁷ *R. parkeri*. Data are representative of 3 independent experiments. The white arrow indicates the injection site on the right flank of the mouse. Scale bar, 1 cm. c) Gross pathology of a human *R. parkeri* infection, from Paddock *et al*⁴. d) Representative images of *Ifnar^{-/-}Ifngr^{-/-}* mice infected intradermally with the indicated amounts of WT *R. parkeri* at 9 d.p.i. Scale bar, 1 cm. Data are representative of two independent experiments.



642

643

644

645

646

647

648

649

650

651

652

653

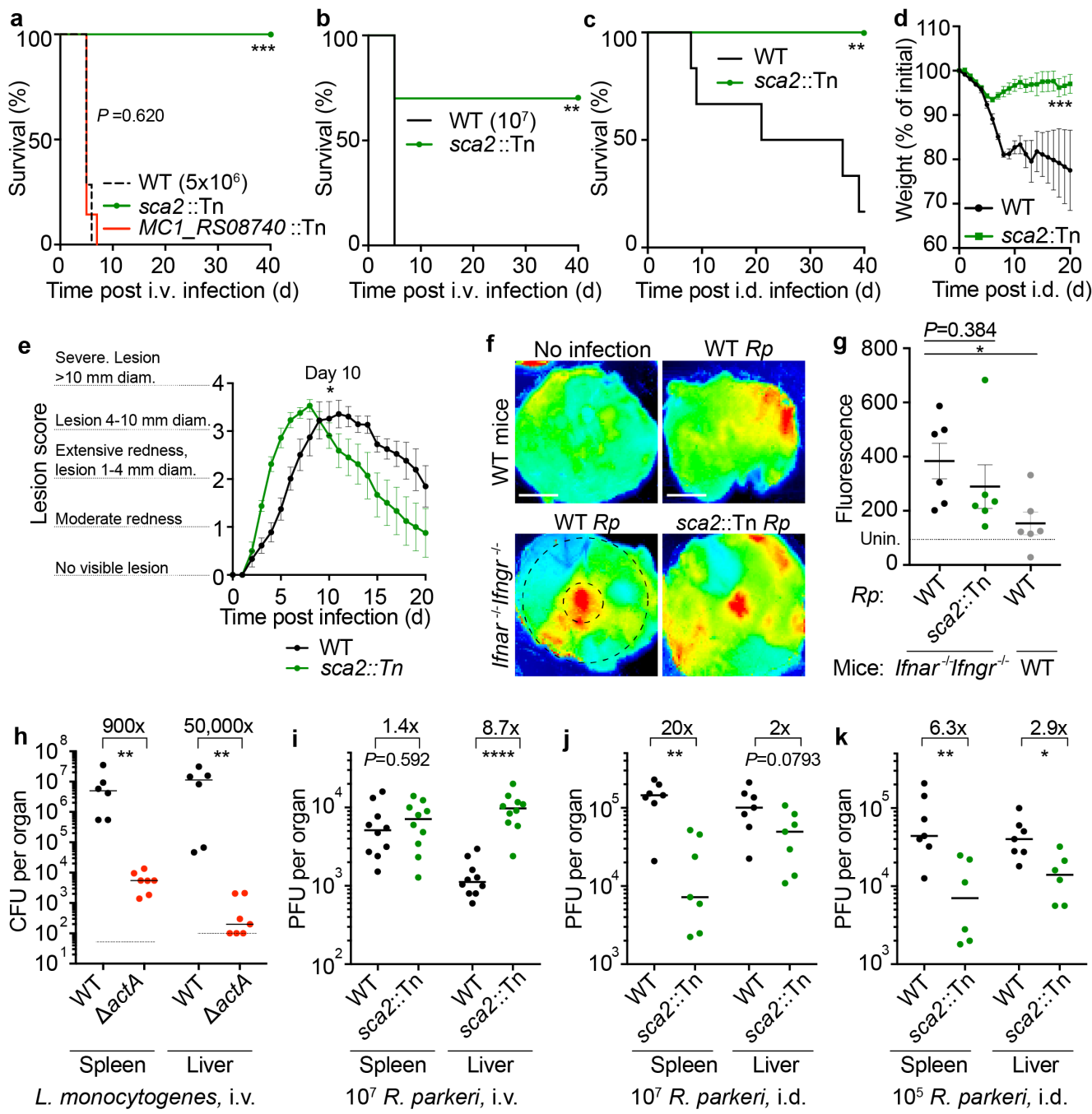
654

Figure 2: I.d. infection of *Ifnar*^{-/-}*Ifngr*^{-/-} mice by *R. parkeri* elicits disseminated, lethal disease.

a) Weight changes over time in mice infected i.d. with *R. parkeri*. Data are shown as a percentage change to initial weight. In the left panel, all mice were infected with 10⁷ *R. parkeri*; n=7 (WT), n=11 (*Ifnar*^{-/-}), n=7 (*Ifngr*^{-/-}), n=9 (*Ifnar*^{-/-}*Ifngr*^{-/-}) and 4 (*Tlr4*^{-/-}) individual mice. In the right panel, *Ifnar*^{-/-}*Ifngr*^{-/-} mice were infected with the indicated amounts of *R. parkeri*; n=7 (10⁵ *R. parkeri*), n=7 (10⁴ *R. parkeri*), n=8 (10³ *R. parkeri*), n=7 (10² *R. parkeri*), n=7 (10¹ *R. parkeri*) individual mice. WT data is the same in both panels. Data for each genotype are combined from two or three independent experiments. b) Temperature changes over time in mice intradermally infected with 10⁷ *R. parkeri*. Each line is an individual mouse. Mice were euthanized if their temperature fell below 90° F, as indicated by the dotted line. Data are the combination of three independent experiments with n=7 (WT) and 9 (*Ifnar*^{-/-}*Ifngr*^{-/-}) individual mice. c) Analysis of gross skin pathology after i.d. infection. *Ifnar*^{-/-}*Ifngr*^{-/-} mice were infected with the indicated number of *R. parkeri* and monitored over time. WT mice were infected with 10⁷ *R.*

655 *parkeri*. Data are the combination of three independent experiments for WT and the 10^7 dose in *Ifnar*^{-/-}
656 *Ifngr*^{-/-} mice; data for all other doses are the combination of two independent experiments. $n=9$ (10^7),
657 $n=5$ (10^5), $n=5$ (10^4), $n=8$ (10^3), $n=7$ (10^2), $n=7$ (10^1), and $n=7$ (WT) individual mice. **d**) Mouse survival
658 after i.d. infection with *R. parkeri*. In the left panel, all mice were infected with 10^7 *R. parkeri*; $n=7$ (WT),
659 $n=11$ (*Ifnar*^{-/-}), $n=7$ (*Ifngr*^{-/-}), $n=4$ *Tlr4*^{-/-}, and $n=12$ (*Ifnar*^{-/-}*Ifngr*^{-/-}) individual mice. Data are the combination
660 of three separate experiments for WT, *Ifnar*, and *Ifnar*^{-/-}*Ifngr*^{-/-} and two separate experiments for *Ifngr*^{-/-}
661 and *Tlr4*^{-/-}. In the right panel, *Ifnar*^{-/-}*Ifngr*^{-/-} mice were infected with the indicated amounts of *R. parkeri*.
662 Data are the combination of two independent experiments; $n=7$ (10^5), $n=7$ (10^4), $n=8$ (10^3), $n=7$ (10^2),
663 and $n=7$ (10^1) individual mice. **e**) Bacterial burdens in organs of intradermally infected WT and *Ifnar*^{-/-}
664 *Ifngr*^{-/-} mice. Mice were intradermally inoculated with 10^7 *R. parkeri*, and spleens and livers were
665 harvested and plated for p.f.u. at 72 h.p.i. Dotted lines indicate the limit of detection. Data are the
666 combination of two independent experiments. $n=4$ (WT) and 7 (*Ifnar*^{-/-}*Ifngr*^{-/-}) individual mice. Data in **a**,
667 **c** are the mean \pm SEM. Statistical analyses in **a** used a two-way ANOVA where each group was
668 compared to WT at t=20 d.p.i. Statistical analyses in **c** used a two-way ANOVA at t=20 d.p.i. Statistical
669 analyses in **d** used a log-rank (Mantel-Cox) test to compare *Ifnar*^{-/-} to *Ifnar*^{-/-}*Ifngr*^{-/-} at each dose.
670 Statistical analysis in **e** used a two-tailed Mann-Whitney U test. NS, not significant; ** $P<0.01$;
671 *** $P<0.001$; **** $P<0.0001$.
672

673
674



675

676 **Figure 3: *R. parkeri* Sca2 contributes to dissemination from skin to spleens and livers.**

677 **a**) Survival of *Ifnar*^{-/-}*Ifngr*^{-/-} mice upon i.v. infection with 5×10^6 *R. parkeri*. $n=7$ (WT), 10 (sca2::Tn), and 7 (MC1_RS08740::Tn) individual mice. Data are the combination of two independent experiments. **b**) Survival of *Ifnar*^{-/-}*Ifngr*^{-/-} mice upon i.v. infection with 10^7 *R. parkeri*. $n=7$ (WT) and 10 (sca2::Tn) individual mice. Data are the combination of two independent experiments. **c**) Survival of *Ifnar*^{-/-}*Ifngr*^{-/-} mice upon i.d. infection with 10^7 *R. parkeri*. $n=6$ (WT) and 8 (sca2::Tn) individual mice. Data are the combination of two independent experiments. **d**) Weight changes of *Ifnar*^{-/-}*Ifngr*^{-/-} mice upon i.d. infection with 10^7 *R. parkeri*. $n=6$ (WT) and 8 (sca2::Tn) individual mice. Data are the combination of two independent experiments. **e**) Analysis of gross skin pathology after i.d. infection. *Ifnar*^{-/-}*Ifngr*^{-/-} mice were infected with 10^7 of the indicated strains of *R. parkeri* and monitored over time. $n=9$ (WT) and 8 (sca2::Tn) individual mice. Data are the combination of two independent experiments. **f**) Representative images of fluorescence in mouse skin after i.d. infection with 10^6 *R. parkeri* and delivery of a fluorescent tracer. Panels show WT mice, WT *Rp*, *sca2::Tn Rp*, and *Ifnar*^{-/-}*Ifngr*^{-/-} mice.

678 **g**) Fluorescence analysis of skin after i.d. infection with 10^6 *R. parkeri* and delivery of a fluorescent tracer. $n=6$ (WT), 8 (sca2::Tn), and 7 (WT) mice. $P=0.384$. * indicates $P < 0.05$.

679 **h**) CFU per organ of *L. monocytogenes* i.v. infected WT and Δ actA mice. $n=9$ (WT) and 8 (Δ actA) mice. $900x$ and $50,000x$ magnification. ** indicates $P < 0.01$.

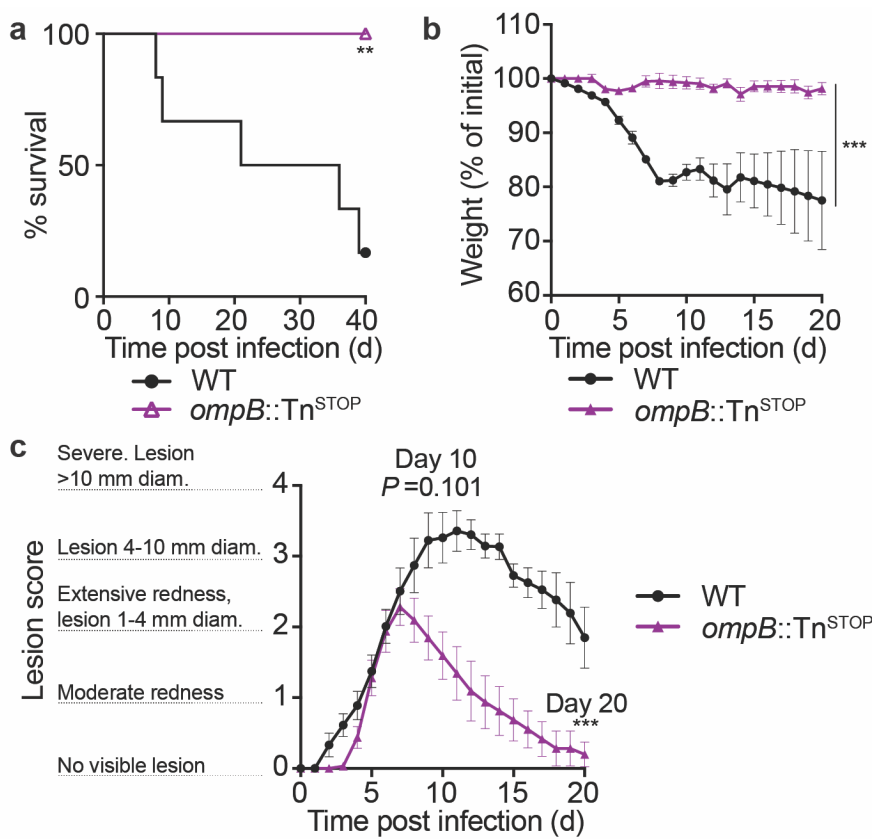
680 **i**) PFU per organ of 10^7 *R. parkeri* i.v. infected WT and *sca2::Tn* mice. $n=6$ (WT) and 8 (*sca2::Tn*) mice. $1.4x$ and $8.7x$ magnification. $P=0.592$. **** indicates $P < 0.0001$.

681 **j**) PFU per organ of 10^7 *R. parkeri* i.d. infected WT and *sca2::Tn* mice. $n=6$ (WT) and 8 (*sca2::Tn*) mice. $20x$ and $2x$ magnification. $P=0.0793$.

682 **k**) PFU per organ of 10^5 *R. parkeri* i.d. infected WT and *sca2::Tn* mice. $n=6$ (WT) and 8 (*sca2::Tn*) mice. $6.3x$ and $2.9x$ magnification. ** indicates $P < 0.01$ and * indicates $P < 0.05$.

683
684
685
686
687

688 dextran, at 5 d.p.i. Scale bars, 1 cm. The larger black dashed circle represents the area that was
689 measured for fluorescence for each sample, as indicated in **Fig. 3g** (~80,000 pixels). The smaller black-
690 dashed circle represents of the injection site area that was measured for fluorescence for each sample,
691 as indicated in **Fig. S3** (~7,800 pixels). **g)** Quantification of fluorescence in mouse skin after i.d.
692 infection. Mice were infected with 10^7 *R. parkeri*, and 150 μ l fluorescent dextran was intravenously
693 delivered at 5 d.p.i. Skin was harvested 2 h later, and fluorescence was measured using a fluorescence
694 imager. Data indicate measurements of larger areas of skin, as indicated in **f** by the larger black circle.
695 $n=6$ (WT *R. parkeri*) and $n=6$ (*sca2::Tn R. parkeri*) individual *Ifnar*^{-/-}*Ifngr*^{-/-} mice; $n=6$ (WT *R. parkeri*)
696 individual WT mice. For each experiment, the average of uninfected samples was normalized to 100;
697 each sample was divided by the average for uninfected mice and multiplied by 100; the dotted horizontal
698 line indicates 100 arbitrary units, corresponding to uninfected (unin.) mice. Data are the combination of
699 two independent experiments. **h)** Quantification of *L. monocytogenes* abundance in organs of WT
700 C57BL/6J mice upon i.v. infection with 10^4 bacteria, at 72 h.p.i. Data are the combination of two
701 independent experiments. $n=6$ (WT), $n=7$ (Δ *actA*) individual mice. **i)** Quantification of *R. parkeri*
702 abundance in spleens and livers of WT C57BL/6J mice upon i.v. infection, at 72 h.p.i. Data are the
703 combination of two independent experiments. $n=10$ (WT) and 10 (*Sca2::Tn*) individual mice. **j)**
704 Quantification of *R. parkeri* abundance in organs upon i.d. infection with 10^7 *R. parkeri*. $n=7$ (WT) and
705 7 (*sca2::Tn*) individual mice. Data are the combination of two independent experiments. Data for WT *R.*
706 *parkeri* in *Ifnar*^{-/-}*Ifngr*^{-/-} mice are the same as in **Fig. 2e**. **k)** Quantification of *R. parkeri* abundance in
707 organs upon i.d. infection with 10^5 *R. parkeri*. $n=7$ (WT) and 6 (*sca2::Tn*). Data are the combination of
708 two independent experiments. Solid horizontal bars in **g** indicate means; solid horizontal bars in **h-k**
709 indicate medians; error bars indicate SEM. Statistical analyses for survival in **a, b, c** used a log-rank
710 (Mantel-Cox) test. Statistical analysis in **d** used a two-way ANOVA at t=20. Statistical analysis in **e** used
711 a two-way ANOVA from 0 to 10 d.p.i. Statistical analyses in **g** used a two-tailed Student's T test.
712 Statistical analyses in **h, i, j, k** used a two-tailed Mann-Whitney U test. The fold change in **h, i, j, k**
713 indicates differences of medians. * $P<0.05$; ** $P<0.01$; *** $P<0.001$; **** $P<0.0001$.



714

715

716

717

718

719

720

721

722

723

724

725

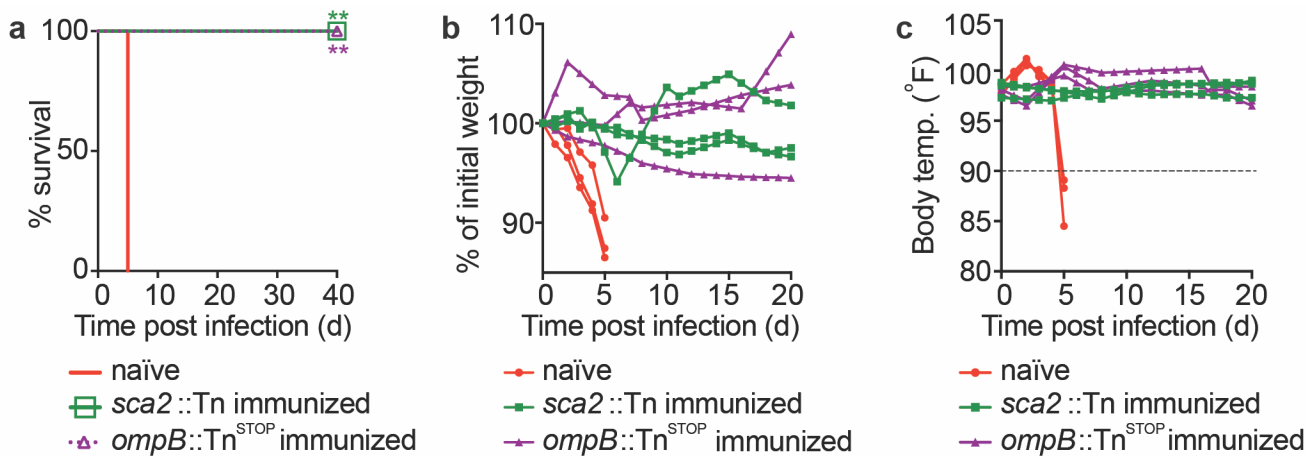
726

727

Figure 4: *ompB* mutant *R. parkeri* elicit no lethality and reduced skin lesion formation in *Ifnar*^{-/-} *Ifngr*^{-/-} mice.

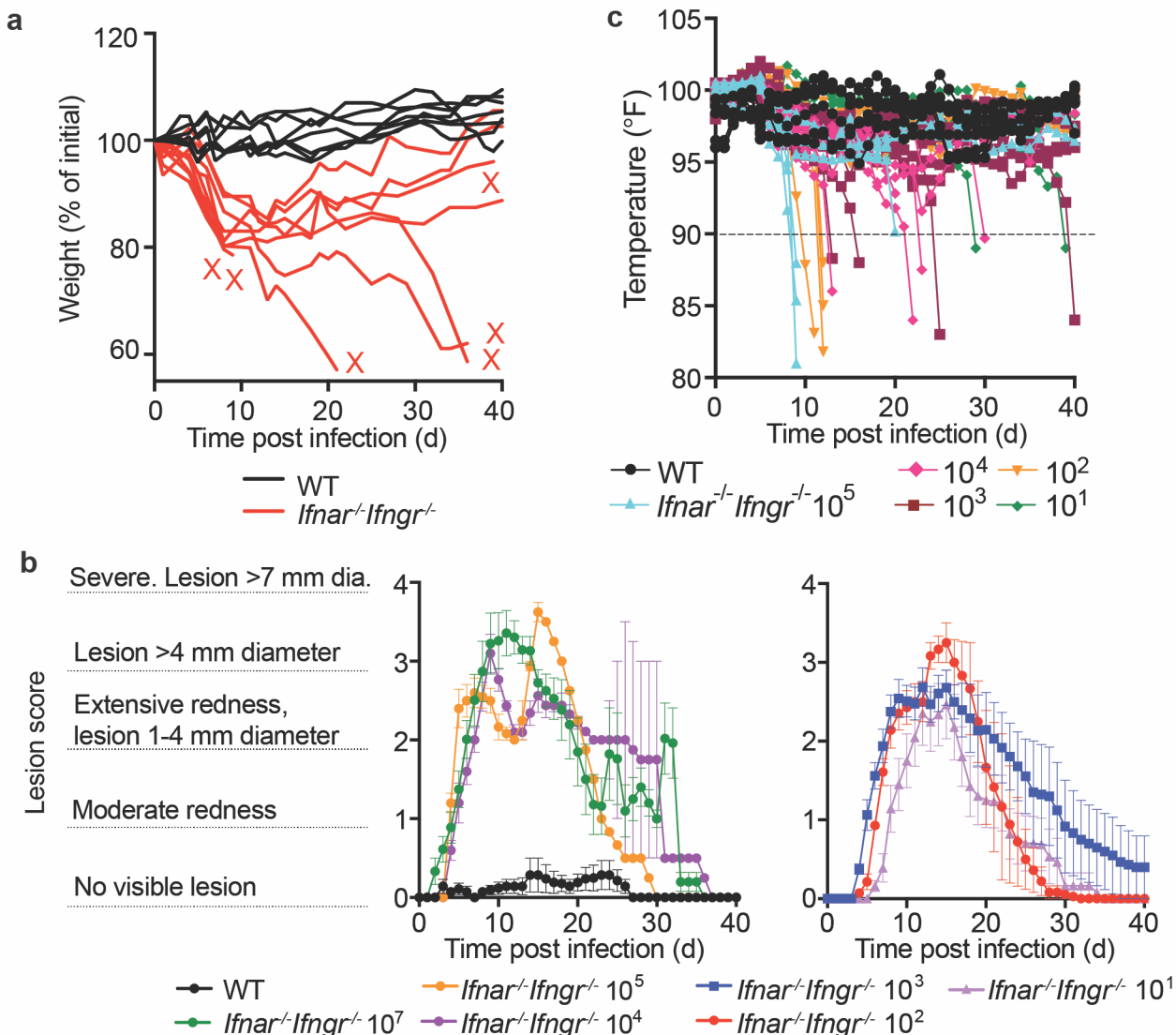
a) Survival of *Ifnar*^{-/-} *Ifngr*^{-/-} mice upon i.d. infection with 10⁷ *R. parkeri*. n=6 (WT) and 8 (*ompB*::Tn^{STOP}) individual mice. Data are the combination of two independent experiments. Data for WT are the same as in Fig. 3c. b) Weight changes of *Ifnar*^{-/-} *Ifngr*^{-/-} mice upon i.d. infection with 10⁷ *R. parkeri*. n=6 (WT) and 8 (*ompB*::Tn^{STOP}) individual mice. Data are the combination of two independent experiments. Data for WT are the same as in Fig. 3d. c) Analysis of gross skin pathology after i.d. infection. *Ifnar*^{-/-} *Ifngr*^{-/-} mice were infected with 10⁷ of the indicated strains of *R. parkeri* and monitored over time. n=9 (WT) and 8 (*ompB*::Tn^{STOP}) individual mice. Data are the combination of two independent experiments. Data for WT are the same as in Fig. 3e. Error bars indicate SEM. Statistical analyses in a used a log-rank (Mantel-Cox) test. Statistical analysis in b used a two-way ANOVA from 0 to 20 d.p.i. **P<0.01; ***P<0.001.

728



a) Survival of immunized and naïve *Ifnar*^{-/-}*Ifngr*^{-/-} mice upon i.v. *R. parkeri* infection. Immunized mice were first infected with 5×10^6 *sca2*::Tn or 10^7 *ompB*::Tn^{STOP} *R. parkeri* and were re-challenged 40 d later with 10^7 WT *R. parkeri*. $n=6$ (naïve); $n=5$ (*sca2*::Tn immunized); $n=5$ (*ompB*::Tn^{STOP} immunized) individual mice. Data are the combination of two independent experiments. b) Weight changes over time in mice infected i.d. with 10^7 *R. parkeri*. Data are representative of two independent experiments. $n=3$ (naïve); $n=3$ (*sca2*::Tn immunized); $n=3$ (*ompB*::Tn^{STOP} immunized) individual mice. Each line represents an individual mouse. c) Temperature changes over time in mice infected i.d. with 10^7 *R. parkeri*. Data are representative from two independent experiments. $n=3$ (naïve); $n=3$ (*sca2*::Tn immunized); $n=3$ (*ompB*::Tn^{STOP} immunized) individual mice. Each line represents an individual mouse. Statistical analyses in a used a log-rank (Mantel-Cox) test to compare each group of immunized mice to naïve mice. ** $P<0.01$.

754



755

756

757

758

759

760

761

762

763

764

765

766

767

768

769

770

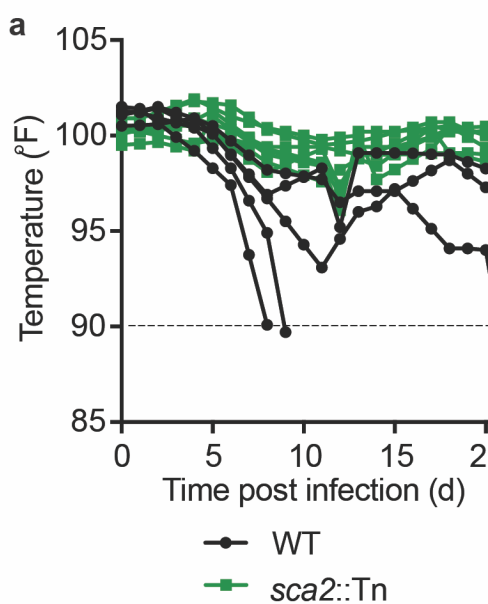
771

772

773

Figure S2: Ifnar^{-/-} or Ifngr^{-/-} mice develop limited disease upon intradermal infection, and Ifnar^{-/-} Ifngr^{-/-} develop lesions of dose-dependent severity.

a) Weight changes over time in mice intradermally infected with 10^7 WT *R. parkeri*. Data are the combination of two independent experiments for WT and three for Ifnar^{-/-}/Ifngr^{-/-}; $n=7$ (WT) and $n=9$ (Ifnar^{-/-}/Ifngr^{-/-}) individual mice. Each line is an individual mouse. b) Gross pathological analysis of the skin infection site after i.d. infection. Ifnar^{-/-}/Ifngr^{-/-} mice were infected with the indicated number of *R. parkeri* and monitored over time. Data are the combination of three independent experiments for the 10^7 dose and two independent experiments for all other doses. $n=7$ (WT), $n=9$ (10^7), $n=5$ (10^5), $n=5$ (10^4), $n=8$ (10^3), $n=7$ (10^2), and $n=7$ (10^1) individual mice. Data are the same as in Fig. 2c but are extended to 40 d.p.i. Data are represented as means and error bars indicate SEM. c) Temperature changes over time in mice infected i.d. with the indicated amounts of WT *R. parkeri*. Data are the combination of two independent experiments; $n=7$ (WT), $n=7$ (10^5), $n=7$ (10^4), $n=8$ (10^3), $n=7$ (10^2), and $n=7$ (10^1) individual mice. Each bar represents an individual mouse. Mice were euthanized if their body temperature fell below 90° F, as indicated by the dotted line.



774
775 **Figure S3: Intradermal infection of *Ifnar*^{-/-}*Ifngr*^{-/-} mice with *sca2::Tn* *R. parkeri* causes less severe**
776 **temperature loss as compared to WT bacteria.**

777 a) Temperature changes over time in mice infected i.d. with 10^7 *R. parkeri*. Data are the combination of
778 two independent experiments; $n=5$ (WT), $n=8$ (sca2::Tn) individual mice. Each line represents an
779 individual mouse. Mice were euthanized if their body temperature fell below 90° F, as indicated by the
780 dotted line.

781

782

783

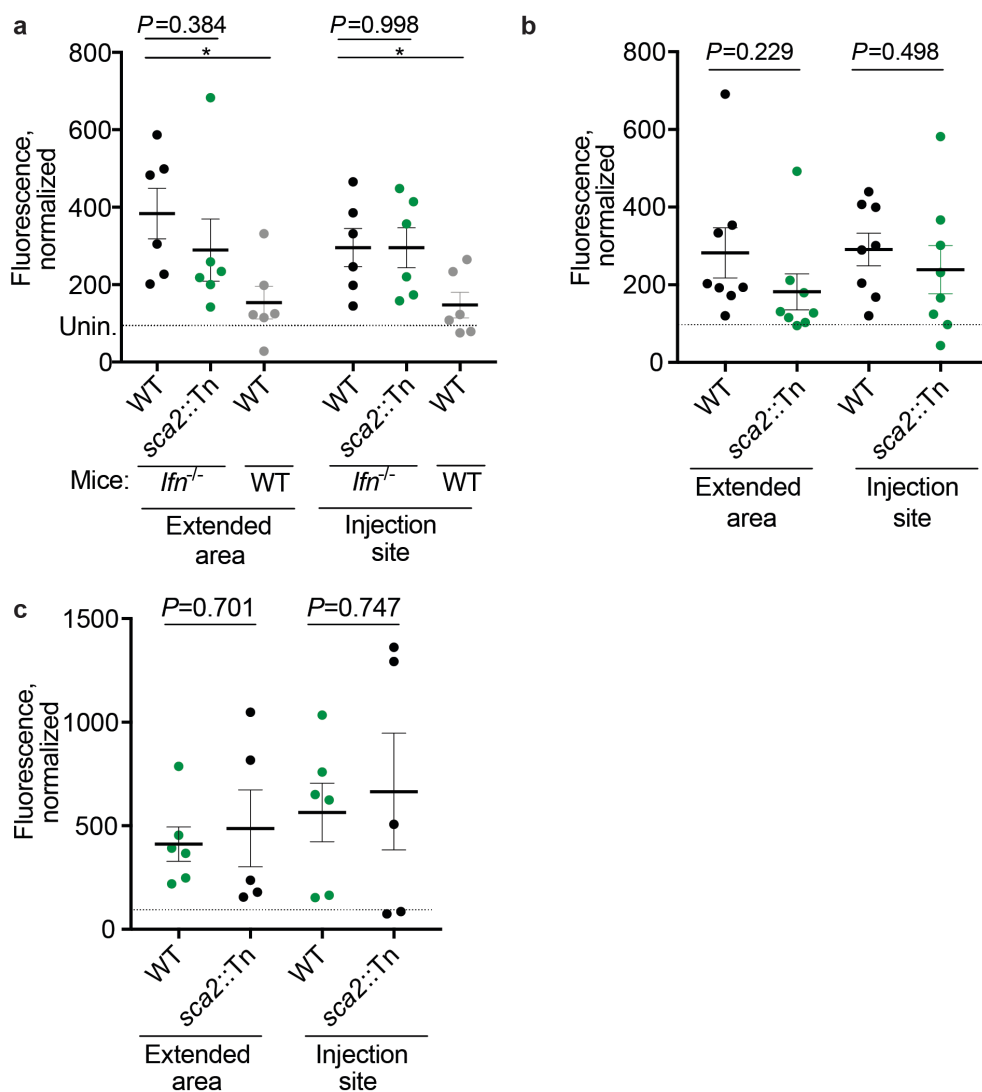
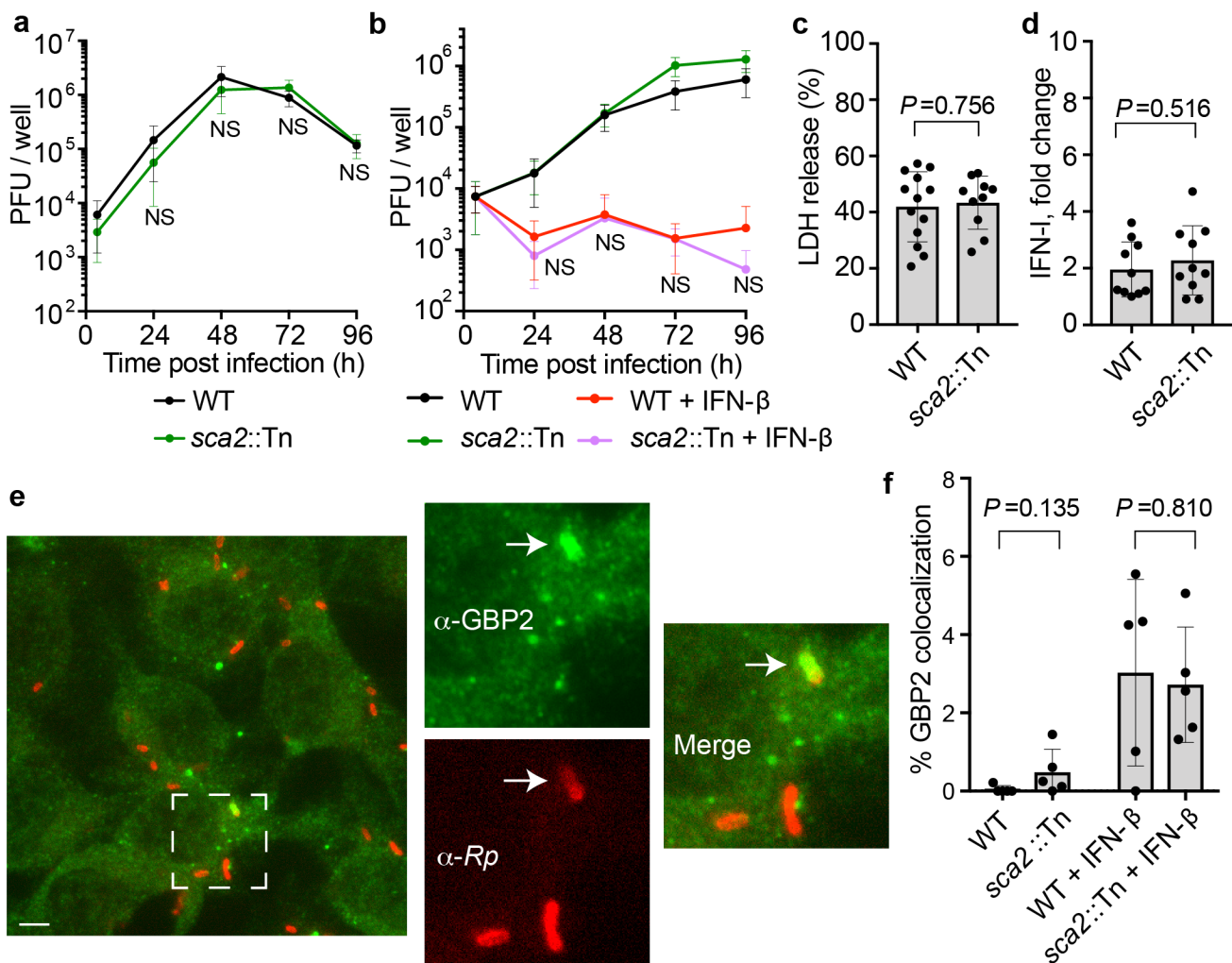


Figure S4: WT and sca2::Tn *R. parkeri* elicit similar amounts of vascular damage in skin upon i.d. infection of *Ifnar*^{-/-}/*Ifngr*^{-/-} mice.

a) Quantification of fluorescence in mouse skin after i.d. infection. Mice were infected i.d. with 10^7 *R. parkeri* and fluorescent dextran was intravenously delivered at 5 d.p.i. Skin was harvested 2 h after delivery of dextran and analyzed with a fluorescence imager. $n=6$ (WT *R. parkeri*) and $n=6$ (sca2::Tn *R. parkeri*) individual *Ifnar*^{-/-}/*Ifngr*^{-/-} mice; $n=6$ (WT *R. parkeri*) individual WT mice. Data in the 'extended area' are the same as those reported in **Fig. 3e**. b) Quantification of fluorescence in mouse skin after i.d. infection. Mice were infected i.d. with 10^6 *R. parkeri*, and fluorescent dextran was intravenously delivered at 5 d.p.i. Skin was harvested 2 h after delivery of dextran and analyzed with a fluorescence imager. $n=8$ (WT *R. parkeri*) and $n=8$ (sca2::Tn *R. parkeri*) individual *Ifnar*^{-/-}/*Ifngr*^{-/-} mice. c) Quantification of fluorescence in mouse skin after i.d. infection. Mice were infected i.d. with 10^5 *R. parkeri* and fluorescent dextran was intravenously delivered at 5 d.p.i. Skin was harvested 2 h after delivery of dextran and analyzed with a fluorescence imager. $n=6$ (WT *R. parkeri*) and $n=5$ (sca2::Tn *R. parkeri*) individual *Ifnar*^{-/-}/*Ifngr*^{-/-} mice. For each experiment, the average of uninfected samples was normalized to 100, and each sample was divided by the average for uninfected mice and multiplied by 100; the dotted horizontal line indicates 100 arbitrary units, corresponding to uninfected (unin.) mice. Representative sizes for the larger 'extended areas' of skin and the smaller 'injection site' areas of skin are indicated in **Fig. 3d**. Data are each the combination of two independent experiments. Solid horizontal bars indicate means; error bars indicate SEM. For statistical analyses, a two-tailed Student's T test was used to compare the indicated samples.



806

807 **Figure S5: Sca2 does not significantly enhance *R. parkeri* avoidance of antibacterial innate**
 808 **immune responses *in vitro*.**

809 **a)** *R. parkeri* abundance in HMEC-1s, multiplicity of infection (MOI) of 0.2. Data are the combination of
 810 three independent experiments, each with two biological replicates. For statistics, a two-tailed
 811 Student's T test was used to compare WT to *sca2::Tn* at 48, 72, and 96 h.p.i. No statistically
 812 significant differences were observed at any time. **b)** *R. parkeri* abundance in BMDMs, MOI of 1. Data
 813 are the combination of three independent experiments, each with two biological replicates. Data were
 814 normalized by multiplying fold difference between WT and *Sca2::Tn* at 4 h.p.i. to *Sca2::Tn* and
 815 *Sca2::Tn + IFN-β* data at all time points. **c)** Host cell death upon *R. parkeri* infection of BMDMs, as
 816 measured by lactate dehydrogenase (LDH) release assay, MOI of 1. From left to right, $n=6$ and 3
 817 biological replicates and are the combination of two independent experiments. **d)** IFN-I abundance in
 818 supernatants of infected BMDMs (24 h.p.i.; MOI of 1), measured using a luciferase reporter assay.
 819 The data show the fold change over uninfected cells. $n=7$ and 7 biological replicates and are the
 820 combination of two independent experiments. **e)** A representative image using x100 confocal
 821 immunofluorescence microscopy of WT BMDMs infected with *sca2::Tn R. parkeri* in the presence of
 822 100 U recombinant IFN-β (3 h.p.i.; MOI of 1). Green, $α$ -GBP2; red, $α$ -*Rickettsia* (*Rp*). The dotted
 823 square indicates the image that is expanded in the other images, separated into two individual and
 824 one merged channel. Scale bars, 2.5 $μ$ m. White arrows indicate a bacterium that colocalizes with
 825 GBP2. Data are representative of three independent experiments. **f)** Quantification of GBP2
 826 colocalization with *R. parkeri* in BMDMs at 24 h.p.i. Each data point is an average of at least five
 827 separate images totaling >150 bacteria. Data are the combination of three independent experiments.
 828 Statistical analyses used a two-tailed Student's T test. NS, not significant. Data in **a, b** are means; bars
 829 in **c, d**, and **f** are means; error bars indicate SD.